

FUELING ACTIVE GALACTIC NUCLEI. II. SPATIALLY RESOLVED MOLECULAR INFLOWS AND OUTFLOWS

R. I. DAVIES¹, W. MACIEJEWSKI², E. K. S. HICKS^{3,4}, E. EMSELLEM⁵, P. ERWIN^{1,6}, L. BURTSCHER¹, G. DUMAS⁷, M. LIN¹, M. A. MALKAN⁸, F. MÜLLER-SÁNCHEZ⁹, G. ORBAN DE XIVRY¹, D. J. ROSARIO¹, A. SCHNORR-MÜLLER¹, AND A. TRAN⁴

¹ Max-Planck-Institute für Extraterrestrische Physik, Postfach 1312, D-85741 Garching, Germany

² Astrophysics Research Institute, Liverpool John Moores University, IC2 Liverpool Science Park, 146 Brownlow Hill, L3 5RF, UK

³ Astronomy Department, University of Alaska, Anchorage, Alaska 99508, USA

⁴ Department of Astronomy, University of Washington Seattle, WA 98195, USA

⁵ European Southern Observatory, Karl-Schwarzschild Str. 1, D-85748 Garching, Germany

⁶ Universitäts-Sternwarte München, Scheinerstrasse 1, D-81679 München, Germany

⁷ Institut de Radio Astronomie Millimétrique (IRAM), 300 Rue de la Piscine, Domaine Universitaire, F-38406 Saint Martin d'Herès, France

⁸ Astronomy Division, University of California, Los Angeles, CA 90095-1562, USA

⁹ Center for Astrophysics and Space Astronomy, University of Colorado, Boulder, CO 80309-0389, USA

Received 2014 March 28; accepted 2014 July 9; published 2014 August 21

ABSTRACT

We analyze the two-dimensional distribution and kinematics of the stars as well as molecular and ionized gas in the central few hundred parsecs of five active and five matched inactive galaxies. The equivalent widths of the Br γ line indicate that there is no ongoing star formation in their nuclei, although recent (terminated) starbursts are possible in the active galaxies. The stellar velocity fields show no signs of non-circular motions, while the 1-0 S(1) H₂ kinematics exhibit significant deviations from simple circular rotation. In the active galaxies the H₂ kinematics reveal inflow and outflow superimposed on disk rotation. Steady-state circumnuclear inflow is seen in three active galactic nuclei (AGNs), and hydrodynamical models indicate it can be driven by a large-scale bar. In three of the five AGNs, molecular outflows are spatially resolved. The outflows are oriented such that they intersect, or have an edge close to, the disk, which may be the source of molecular gas in the outflow. The relatively low speeds imply the gas will fall back onto the disk, and with moderate outflow rates, they will have only a local impact on the host galaxy. H₂ was detected in two inactive galaxies. These exhibit chaotic circumnuclear dust morphologies and have molecular structures that are counter-rotating with respect to the main gas component, which could lead to gas inflow in the near future. In our sample, all four galaxies with chaotic dust morphology in the circumnuclear region exist in moderately dense groups with 10–15 members where accretion of stripped gas can easily occur.

Key words: galaxies: active – galaxies: ISM – galaxies: kinematics and dynamics – galaxies: nuclei – galaxies: Seyfert – infrared: galaxies

Online-only material: color figures

1. INTRODUCTION

This paper is the second part of a project to study the molecular gas and stellar properties in the circumnuclear region of five matched pairs of nearby active and inactive galaxies. The rationale for embarking on this project was that, despite the statistical studies of correlations between active galactic nucleus (AGN) and host galaxy properties (e.g., Kauffmann et al. 2003; Cid Fernandes et al. 2004; Ho 2008; Schawinski et al. 2010; Koss et al. 2011, see also other references below), there is no consensus on the mechanisms that drive gas to the nuclear region. We aim to identify which structural and kinematic properties of the stars and molecular gas are present in active, but absent in inactive, galaxies, and hence may be related to fueling AGNs. Hicks et al. (2013; hereafter Paper I) report on systematic differences within the central few hundred parsecs: with respect to inactive galaxies, hosts of Seyfert nuclei have more centrally concentrated surface brightness profiles for both stellar continuum and H₂ 1-0 S(1) emission, as well as lower stellar velocity dispersions and elevated H₂ 1-0 S(1) luminosity. These results suggested that Seyfert galaxies have a nuclear structure that is dynamically colder than the bulge, and comprises a significant gas reservoir together with a relatively young stellar population. In this paper, we focus on the spatially resolved stellar and molecular gas kinematics, with a goal to

trace inflow mechanisms working on these scales. As such, we distinguish between the following mechanisms that might lead to gas inflow and ultimately to accretion onto the central massive black hole: (1) major merger, the coalescence of two approximately equally massive galaxies; (2) minor merger, the accretion of a small galaxy such as a dwarf into a larger one (i.e., coalescence of very unequal mass galaxies); (3) accretion of gas streamers (i.e., intergalactic atomic or molecular gas, perhaps in the form of spurs or bridges), which might originally have been produced during a merger or interaction, perhaps between other galaxies; (4) secular evolution, which is inflow of gas due to long-lasting disk-driven processes, perhaps (but not necessarily) stimulated originally by an interaction.

There have been a large number of studies addressing at least some of these issues, focusing in particular on the role of major mergers. While there are differences in the selection (e.g., hard X-ray or mid-infrared), the luminosity range (typically from 10^{41} – 10^{42} erg s⁻¹ to 10^{44} – 10^{45} erg s⁻¹), the redshift range (from $z = 0$ to 3), and the technique used to identify mergers (e.g., close pairs or disturbed hosts), a clear consensus is emerging that major mergers appear to play a relatively minor role in triggering AGN activity (e.g., Kocevski et al. 2012; Schawinski et al. 2012; Karouzos et al. 2014; Villforth et al. 2014). A similar conclusion is reached when looking at the star formation rates: typical QSOs at $z \sim 2$ lie in galaxies with normal, rather than

enhanced, star formation rates (Rosario et al. 2013). Only above $L_{\text{AGN}} \sim 10^{45} \text{ erg s}^{-1}$ is there some observational evidence that major mergers may begin to dominate AGN triggering (Treister et al. 2012; Rosario et al. 2012). With respect to low and intermediate luminosity AGNs, Neistein & Netzer (2014) argue that they may be triggered mostly by minor mergers, and, at least for early type galaxies, Simões Lopes et al. (2007) and Martini et al. (2013) suggest that external accretion, perhaps in the form of minor mergers, may be fueling the nuclear activity. Beyond finding that about half of AGNs are in disk hosts and also that about half of AGNs have hosts that appear undisturbed (Kocevski et al. 2012), the observational studies above cannot probe further into the relative roles of minor mergers, gas accretion, or secular evolution. Clues to their roles may lie in the local environment of the AGN. For example, Arnold et al. (2009) found that the fraction of X-ray-selected AGNs in groups is a factor two higher than in clusters, and Georgakakis et al. (2008) showed that X-ray AGNs are more frequently found in groups than in the field.

A difficulty with all statistical studies, especially in the context of a control sample, is the transient nature of AGN activity. The timescale on which it occurs is expected to be short, characteristically of order 100 Myr, and during this time it can flicker on and off with a timescale of 1–10 Myr due to stochasticity at small scales (Haehnelt & Rees 1993; Ulrich et al. 1997; Novak et al. 2011; Hickox et al. 2014; Neistein & Netzer 2014). Indeed, Keel et al. (2012) and Schirmer et al. (2013) report AGN light echoes that suggest variability on even shorter timescales is possible. In these galaxies, illumination of the very extended narrow line region requires a recent AGN luminosity significantly greater than that now inferred, implying that the AGN has decreased in luminosity by 1–2 orders of magnitude on a timescale of 0.1 Myr. In comparison, the timescale on which a merger occurs can be measured in Gyr (Lotz et al. 2008). Even for compact groups that evolve rapidly, the timescale over which the group survives (i.e., the galaxies have not yet all merged together) is measurable in Gyr (Barnes 1989). A similar mismatch in timescales is also an issue when investigating links between AGNs and host galaxy morphological structures. For example, despite much effort, there is at best only marginal evidence for a direct link between bars and AGNs (Shlosman et al. 2000; Laine et al. 2002; Laurikainen et al. 2004; Cisternas et al. 2013), although there is a strong indirect link for at least one subset of AGNs (Orban de Xivry et al. 2011). Looking in more detail for links between Seyferts and their host galaxies, Hunt & Malkan (2004) found no significant differences in the presence of circumnuclear bars, boxy and disk isophotes, or other non-axisymmetric features in a comparison of matched samples of Seyferts and inactive galaxies. They do, however, report that Seyferts are more likely to show isophotal twisting, suggesting a potential increase in the disturbance of the kinematics in these active galaxies (and noting that this is driven by the Seyfert 2s in their sample). When looking at their data, we find that this difference is occurring equally in both early and late type hosts. We also find that there is a higher fraction of late type inactive galaxies than late type Seyferts with circumnuclear bars, the implications of which are not clear.

In this work, we attempt to overcome the difficulties due to mismatched timescales by focusing on the mechanisms operating in the central few hundred parsecs of active and inactive galaxies. Here, where the orbital velocities are $100\text{--}150 \text{ km s}^{-1}$ at a radius of 100 pc (see Paper I), the dynamical timescales are 2–3 Myr, comparable to the AGN duty cycle (i.e., the timescale

for order-of-magnitude variability in accretion rate) mentioned above.

Previous studies of matched active and inactive galaxy samples based on optical integral field spectroscopy, such as Dumas et al. (2007) and Westoby et al. (2012) which we discuss in Section 8, have tended to focus on larger scales, from a few kpc down to their resolution limit of 100–200 pc (or more typically 600 pc in the latter study). The seeing under which our data were taken have enabled us to achieve resolutions of ~ 50 pc, and we probe specifically the circumnuclear region out to radii of only a few hundred parsecs. With respect to the optical regime, observing in the near-infrared around $2 \mu\text{m}$ provides two advantages. It enables us to probe to greater optical depth ($A_K \sim 0.1 A_V$); and our spectral range includes the H_2 1-0 S(1) line which directly traces molecular gas at ~ 2000 K, in addition to the $\text{Br}\gamma$ line that probes the ionized phase. We combine this with the stellar distribution and kinematics traced through the CO 2-0 bandhead.

This paper is organized as follows, beginning with a short recap of the sample in Section 2. In Section 3, we look at the environment of the host galaxies since this is fundamental to the later discussion. Using the galaxy orientations adopted in the Appendix, Section 4 assesses whether a simple dynamical model is an appropriate prescription for, and if there is evidence for perturbations in, the circumnuclear stellar kinematics. Then, in Section 5, we make a detailed analysis of the H_2 1-0 S(1) distribution and kinematics. We bring the results on the individual galaxies together in Sections 6 and 7 where we discuss the evidence for and against nuclear star formation, and the properties of the observed molecular outflows. Finally, in Section 8, we broaden our discussion to address evidence for internal secular driven inflow versus external accretion, and the role of environment and host galaxy type. We do this not only in the context of our sample, but also other samples with spatially resolved stellar and gas kinematics, and also with reference to H I studies. We summarize our conclusions in Section 9.

2. SAMPLE

This paper focuses on a small sample that was selected as matched pairs of active and inactive galaxies. However, our analysis does not treat them as such. We assess them first as an active sample and an inactive sample; and then as a combined sample of which some members are active and some are inactive. The targets were already discussed in Paper I, where a full description of the sample selection and properties is given, together with a discussion of the observations and data reduction. Here, Table 1 summarizes the galaxy properties and Table 2 provides an overview of the measured line and continuum luminosities. Below we discuss a few key points of the targets and sample.

The observations were obtained with SINFONI, performing K -band integral field spectroscopy in seeing (at the same wavelength) of $0\prime.57 \pm 0\prime.06$. The targets were a subset of five matched pairs of active and inactive galaxies at distances of 10–32 Mpc, taken from the sample of Martini et al. (2003) who published $V - H$ dust structure maps of the circumnuclear region of all the objects. The original matching was based on the host galaxy Hubble type, B -band luminosity, heliocentric velocity, inclination, and angular size. In our subsample, we performed an additional comparison of the H -band luminosity (as a proxy for stellar mass) and physical size of the disks. For both of these quantities, values for the active galaxies as a whole are

Table 1
Galaxy Sample

Pair	Galaxy	Type ^a	AGN	D (Mpc)	PSF FWHM ($''$)	PSF FWHM (pc)
1	NGC 3227	SABa	Sey 1.5	21	0.55	56
2	NGC 5643	SABc	Sey 2	17	0.49	40
3	NGC 6300	SBb	Sey 2	17	0.48	40
4	NGC 6814	SABbc	Sey 1.5	23	0.51	57
5	NGC 7743	SB0	Sey 2	19	0.54	50
1	IC 5267	SA0/a	no	30	0.61	90
2	NGC 4030	SABc	no	27	0.66	87
3	NGC 3368	SABab	no	11	0.58	30
4	NGC 628	SAC	no	10	0.59	28
5	NGC 357	SB0/a	no	32	0.62	97

Notes. The data here are repeated from Tables 1–3 of Hicks et al. (2013), which should be consulted for original sources, details about the quantities given, and other sample properties.

^a Abbreviated classification taken from the NASA/IPAC Extragalactic Database.

~25% smaller, although this difference is only at the 1σ level of significance.

The nuclear properties of the active and inactive samples were originally based on optical emission line ratios. The difference between our two subsamples was confirmed through their 2–10 keV X-ray luminosities, which are listed in Paper I. The active galaxies are all in the range $5\text{--}200 \times 10^{40} \text{ erg s}^{-1}$; only two of the inactive galaxies have measured hard X-ray luminosities, and these are $<2 \times 10^{39} \text{ erg s}^{-1}$. In addition, Paper I showed that three out of five of the active galaxies exhibit a strong spatially unresolved non-stellar continuum in the K band, associated with hot dust heated by the AGN. This is not seen in any of the inactive galaxies.

3. ENVIRONMENT

Before embarking on our analysis, we first look at the environment of the host galaxies, since this can help with understanding the galaxy structure and also shed light on the origin of the gas feeding the AGN.

The barred galaxy NGC 3227 is in an overdense environment, being part of a group of 13 (Garcia 1993) or 14 (Crook et al. 2007) galaxies with a virial mass of $10^{12.8} M_{\odot}$. The latter authors also include it in a high density contrast (HDC) group of four galaxies, and it is interacting with the dwarf elliptical NGC 3226, which is only 13 kpc away and has the same heliocentric velocity. In addition, Mundell et al. (1995) detected large H I plumes extending 70 kpc north and 30 kpc south of NGC 3227, although NGC 3226 itself was undetected.

With respect to the other active galaxies, NGC 5643, NGC 6814, and NGC 7743 all have undisturbed disks, and none are listed as being in groups by either Crook et al. (2007) or Garcia (1993). However, Katkov et al. (2011) point out that, based on the observations of Duprie & Schneider (1996), NGC 7743 has two massive ($10^{7.8}$ and $10^{8.7} M_{\odot}$) H I rich companions at distances of 46 and 61 kpc with systemic velocities differing by only 100 and 200 km s^{-1} , respectively, from NGC 7743. Thus, while NGC 7743 appears undisturbed, it is not isolated. NGC 6300 also does not show obvious signs of disturbance. Although it is reported by Crook et al. (2007) as being part of a low density contrast (LDC) group with nine members, Karachentseva et al. (2010) classify it not only as an isolated

Table 2
Line and Continuum Luminosities ($2''$ aperture)

Galaxy	H ₂ ($10^4 L_{\odot}$)	Br γ ($10^4 L_{\odot}$)	L_K ($10^4 L_{\odot}$)	EW _{Brγ} (\AA)
NGC 3227	31.1	13.5	23.9	1.4
NGC 5643	16.2	6.0	4.8	1.3
NGC 6300	6.4	0.3	4.7	0.1
NGC 6814	4.5	2.3	8.7	0.5
NGC 7743	6.9	<0.2	7.0	<0.03
IC 5267	5.9	<0.1	12.9	<.004
NGC 4030	<1.4	<0.1	7.3	<0.007
NGC 3368	1.3	<0.1	2.8	<0.003
NGC 628	<0.05	<0.01	0.2	<0.01
NGC 357	<4.7	<0.1	8.4	<0.01

Notes. Br γ equivalent widths are determined using the stellar luminosities after correcting the total K -band luminosity for any non-stellar AGN contribution (i.e., $L_{\text{stellar}} = L_K \times f_{\text{dilution}}$). See text for details.

galaxy based on their analysis of 2MASS sources but without significant neighbors identified in optical images.

Turning to the inactive galaxies, IC 5267 was marked as one of the brightest members of the Grus group of 15 bright galaxies by Sandage (1975), and is included in an LDC group of 11 galaxies with a virial mass of $10^{12.7} M_{\odot}$ by Crook et al. (2007). Within this, it is part of an HDC group of three (Crook et al. 2007) or four (Garcia 1993) galaxies. It has been suggested that it may be interacting with IC 5267A, which lies at a projected distance of 125 kpc, and for which the H I line profiles overlap in velocity range (van Driel et al. 1988). While IC 5267A has hints that it may have been perturbed (although available imaging is too shallow and low resolution to be certain either way), the star forming rings in IC 5267 (Gil de Paz et al. 2007; Grouchy et al. 2010) are very symmetric. Since the primary effect of an interaction is to disturb the outer gas disk, this argues against such a scenario. Instead, it suggests a perturbation propagating outward from the center, perhaps triggered by a companion passing through the center perpendicular to the disk. If that companion was IC 5267A, one might expect IC 5267A to be more disrupted and IC 5267 itself to look more like the Cartwheel galaxy (Struck-Marcell & Higdon 1993; Horellou & Combes 2001). Another cause might be a stream of gas feeding into the central regions of IC 5267, a scenario that is consistent with the group environment but does not necessarily involve IC 5267A. Although the H I image of van Driel et al. (1988) does not show evidence for spurs or other intergalactic gas, it does reveal a significant asymmetric extension of the disk to the southeast.

In contrast, NGC 3368 does show clear evidence for intergalactic H I. It is the brightest member in the Leo group of 12 galaxies (Giuricin et al. 2000), and has also been included in a HDC group of 14 galaxies (within an LDC group of 45 galaxies having a virial mass of $10^{14.0} M_{\odot}$) by Crook et al. (2007), and a group of 9 galaxies by Garcia (1993). It appears to be lying at the end of a gas bridge extending from a large H I structure (Michel-Dansac et al. 2010). Thus, while the outer star forming ring (Gil de Paz et al. 2007) may be associated with the outer Lindblad resonance of the bar, it is also possible that the disk has been perturbed by the intergalactic atomic gas.

The other three inactive galaxies all appear to be undisturbed disk galaxies and, although not isolated, do not reside in massive groups. NGC 357 is not listed as being in a group by either Crook et al. (2007) or Garcia (1993), although van den Bergh (2002)

Table 3
Position Angle

Galaxy	Adopted ^a ($^{\circ}$)	CO Bandheads		Large Scale ^d ($^{\circ}$)
		Kinometry ^b ($^{\circ}$)	Isophotes ^c ($^{\circ}$)	
NGC 3227	155	155	168	159
NGC 5643	-39	-39	-64	-51
NGC 6300	114	114	105	109
NGC 6814	-6	-6	54	15
NGC 7743	-65	-65	-82	-65
IC 5267	-29	19 ^e	-29	-41
NGC 4030	40	40	38	32
NGC 3368	173	173	144	172
NGC 628	... ^f	42 ^d	85	20
NGC 357	-159	-159	-135	-160

Notes. All P.A.s given are the angle east of north for the side with positive velocities (if known). Large-scale P.A.s are typically based on photometry, as described for each galaxy in the [Appendix](#). Where appropriate, the P.A. has been switched by 180° so that it can be compared more easily to the small-scale kinematic P.A.

^a This refers to the P.A. adopted on small scales when fitting disk models; the large-scale values are used to address the uncertainties in direct estimates of the P.A. derived from the small-scale data.

^b Kinometry fit of the 2D CO bandhead velocity and dispersion.

^c Mean P.A. fit to the isophotes of the CO bandhead flux

^d See the [Appendix](#) for details.

^e There is little stellar rotation detected and so the kinometry is poorly constrained.

^f Due to the weak stellar velocity gradient and non-detection of 1-0 S(1) emission, we do not model this galaxy and so have not adopted a P.A.

suggests that, despite it showing no signs of interaction, it is part of a group with at least six other members. NGC 628 and NGC 4030 are reported as being in groups by Garcia (1993) with seven and four members, respectively (the latter being a small group in a southern extension to the Virgo cluster), but do not appear in the listings of Crook et al. (2007). The H I map of NGC 628 also suggests it is undisturbed (Walter et al. 2008).

4. DISK FITS TO STELLAR KINEMATICS

The principal aim of this work is to probe the non-circular motions of the molecular gas traced through the $2.1 \mu\text{m}$ 1-0 S(1) line, once a rotating disk component has been fitted and subtracted. However, it is misleading to make an unconstrained fit of a disk to the H_2 data themselves, since the non-circular motions can be significant. The initial step in our analysis is therefore to independently determine the host galaxy orientation. In the [Appendix](#), we assess the large-scale (i.e., the whole galaxy) orientation, and use this as the context for assessing the apparent orientation from the stellar kinematics and isophotes on small scales (i.e., the few central hundred parsecs within our field of view (FOV)). The three galaxies with notable circumnuclear structure in the stellar continuum are shown in Figure 1. The position angle (P.A.) and inclination (i) for all the galaxies on large and small scales, and also the value we adopt for our analysis, are summarized in Tables 3 and 4. We use these to test whether a simple beam-smearred disk model can provide a good match to the observed stellar velocity field. We do not claim that the stars are in such a disk; indeed Figure 17 of Paper I shows that the circumnuclear stellar distribution traced by the $2.3 \mu\text{m}$ CO bandheads is geometrically thick, although less so for the active galaxies than the inactive ones. The rationale is to (1) determine whether the observed circular stellar velocity can

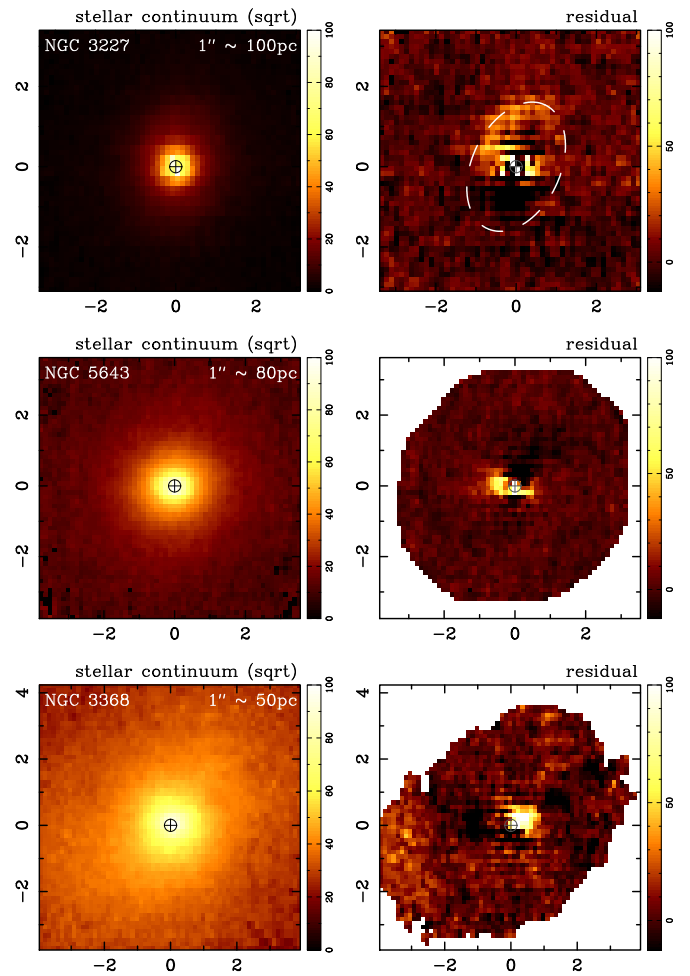


Figure 1. Stellar continuum of three galaxies, together with the residuals after subtracting elliptical isophotes fitted at a single position angle and with a single axis ratio (based on the isophotal values in Tables 3 and 4). These three galaxies have notable circumnuclear structure, which is discussed in Sections 4 and 5, and also in the [Appendix](#). Axis scales are in arcsec, with a conversion to parsec given for each object; north is up and east is left.

(A color version of this figure is available in the online journal.)

be modeled with a simple prescription for the rotation curve, (2) quantify any perturbations to the stellar kinematics, and (3) assess whether we can reasonably apply the same technique to help interpret the more complex H_2 velocity fields in Section 5. We apply the same P.A. and i when fitting a disk model to the gas kinematics, noting that unless there are clear indications to the contrary, and based on kinematics measured in early and late type galaxies (Sarzi et al. 2006; Dumas et al. 2007; Davies et al. 2011; Westoby et al. 2012), our working assumption is that the stellar and molecular gas kinematics are aligned. However, we refer the reader to Section 8 for a discussion of this point.

We make use of the DYSMAL code described in Appendix A of Davies et al. (2011), which was developed to help interpret observations of beam-smearred rotating rings and disks at arbitrary orientations. We keep the number of free parameters to a minimum by fixing the P.A. and i at the values given in Tables 3 and 4, and quantifying the rotation curve in terms of a mass distribution described by a single Sérsic function. This requires three parameters: effective radius, Sérsic index, and scaling. In addition we allow the systemic velocity to vary. The centering is fixed at the peak of the K -band continuum distribution, and the beam-smearing is applied according to the PSF size given in

Table 4
Inclination Angle (Axis Ratio)

Galaxy	Adopted ^a ($^{\circ}$)	CO Bandheads		Large Scale ^d ($^{\circ}$)
		Kinemetry ^b ($^{\circ}$)	Isophotes ^c ($^{\circ}$)	
NGC 3227	47 ^e	41	35	56
NGC 5643	34	34	19	24
NGC 6300	44	44	44	50
NGC 6814	21	43	17	21
NGC 7743	37	37	25	40
IC 5267	40	59 ^f	20	40
NGC 4030	38	38	25	40
NGC 3368	53	22	35	53
NGC 628	... ^g	57 ^f	28	7
NGC 357	37	20	22	37

Notes.

^a This refers to i adopted on small scales when fitting disk models; the large-scale values are used to address the uncertainties in direct estimates i derived from the small-scale data.

^b Kinemetry fit of the 2D CO bandhead velocity and dispersion; these values are associated with a large uncertainty.

^c Mean P.A. fit to the isophotes of the CO bandhead flux.

^d See the [Appendix](#) for details.

^e We have adopted an inclination matching that implied by the circumnuclear ring, as discussed in the [Appendix](#).

^f There is little stellar rotation detected and so the kinemetry is poorly constrained.

^g Due to the weak stellar velocity gradient and non-detection of 1-0 S(1) emission, we do not model this galaxy and so have not adopted any i .

Table 1. The fitting is performed using the Levenberg–Marquardt algorithm as implemented by Markwardt (2009).

The results of the disk fitting process are shown in Figures 2 and 3 for the active and inactive galaxies, respectively. One should be cautious of the apparent striking visual effect that, within the field shown, the inactive galaxies are rotating faster than the active galaxies. This is because we have not plotted—nor modeled—the two inactive galaxies with no measurable rotation. We note that a comparison of the rotation curves, together with the dispersion, is discussed in [Paper I](#).

In most cases the very simple rotation curve provides a fully satisfactory match to the observed velocity field, confirming that we can adopt a similar approach when analyzing the H₂ velocity fields. In a few cases there are measurable residuals. For NGC 7743, these were already compensated for in Figure 2 by including a central compact mass (not necessarily a supermassive black hole, but maybe an unresolved star cluster) to make a steeper velocity gradient in the center while also maintaining an extended mass distribution. The residuals in NGC 3227 are more complex. Since these are anti-symmetric about the center, we conclude that a more detailed prescription for the rotation curve might be more appropriate, perhaps reflecting the impact of a changing mass profile within, and on either side of, the circumnuclear ring shown in Figure 4. We have not attempted to improve on the basic fit because the residuals are at a level of 20–30 km s⁻¹, which is only ~20% of the rotational velocity. In NGC 3368, there are residuals at a similar relatively low level, suggesting that a more complex rotation curve may be required to fit the data more precisely. However, given the low level of the residuals and the additional complexity this brings (especially to the interpretation of the H₂ kinematics in Section 5), we do not feel this is justified.

5. MOLECULAR HYDROGEN

The H₂ velocity fields are much more complex than those of the stars. As such, we adopt a similar approach to fitting disk models as already described for the stellar kinematics, with an additional iteration: initially we use all the data in the fit, but in a second iteration we mask out regions that are obviously anomalous and exclude these from the final fit. This is to reduce any bias from non-circular motions so that they can be better quantified in the residual once the disk model is subtracted. We interpret the residual velocities in conjunction with the H₂ flux maps, and their residuals after subtracting elliptical isophotes. We note that in some cases it is not clear whether a simple disk velocity field is the correct model to subtract, and in two cases we specifically address this by also looking at velocity fields for disks with circumnuclear spirals. By doing so, we take care that our simple approach does not lead to overinterpretation of the velocity residuals.

Table 2 lists the luminosities of the H₂ 1-0 S(1) line as well as those of the Br γ line, extracted in a 2'' diameter aperture. Table 7 summarizes what phenomena and structures we detect in molecular gas, via the 1-0 S(1) lines, in these galaxies, which are described and discussed in detail in the following sub-sections.

5.1. Active Sample

As has been found for other nearby active and inactive galaxies, the 1-0 S(1) distributions and kinematics can show a variety of different phenomena, and vary from being relatively simple to extremely complex (e.g., Davies et al. 2009; Hicks et al. 2009; Müller-Sánchez et al. 2009; Riffel et al. 2009, 2010, 2013; Storchi-Bergmann et al. 2010; Iserlohe et al. 2013; Mazzalay et al. 2014). In our sample the structures exhibited by the AGN typically appear to be a combination of molecular inflow and outflow, superimposed on a rotating disk.

NGC 3227

Large-scale features of NGC 3227, which might have been caused by its interaction with NGC 3226, include a possible bar with bar-induced gas flow. These can be traced inward, and they affect the circumnuclear morphology and kinematics of NGC 3227. In particular, two strings of H α regions, in the form of two spiral arms, can be traced from a radius of 70'' down to a radius of 6'', stretching along a P.A. of -45° in the inner 30'' (see Figure 7 of Mundell et al. 2004). The arms can be traced further inward in molecular gas, where they were earlier reported as a CO bar (Meixner et al. 1990; Mundell et al. 1995), extending to a radius of 7–10'', and stretched along a P.A. of -55° . Inside the bar, Schinnerer et al. (2000) report an asymmetric nuclear ring with diameter of about 3''. This ring is also seen in $J - K$ and $H - K$ color maps constructed from 0''.15 resolution images (Chapman et al. 2000). However, the ring does not show in the $V - H$ HST color map by Martini et al. (2003). This is possibly because of high extinction in the nucleus, and in that case the dust lanes in the *Hubble Space Telescope* (HST) V-band would be a foreground feature. The dust lanes in the $V - H$ HST color map also appear unrelated to the CO bar, which fully fits within the HST field.

Our SINFONI field covers the circumnuclear ring and the area immediately outside it (see Figure 4). The 1-0 S(1) flux distribution, shown in Figure 5, appears elongated along a P.A. between -45° and -50° , which is different from the adopted P.A. = -25° (Table 3). This produces a pattern of positive and negative flux residuals, with the strongest positive residual

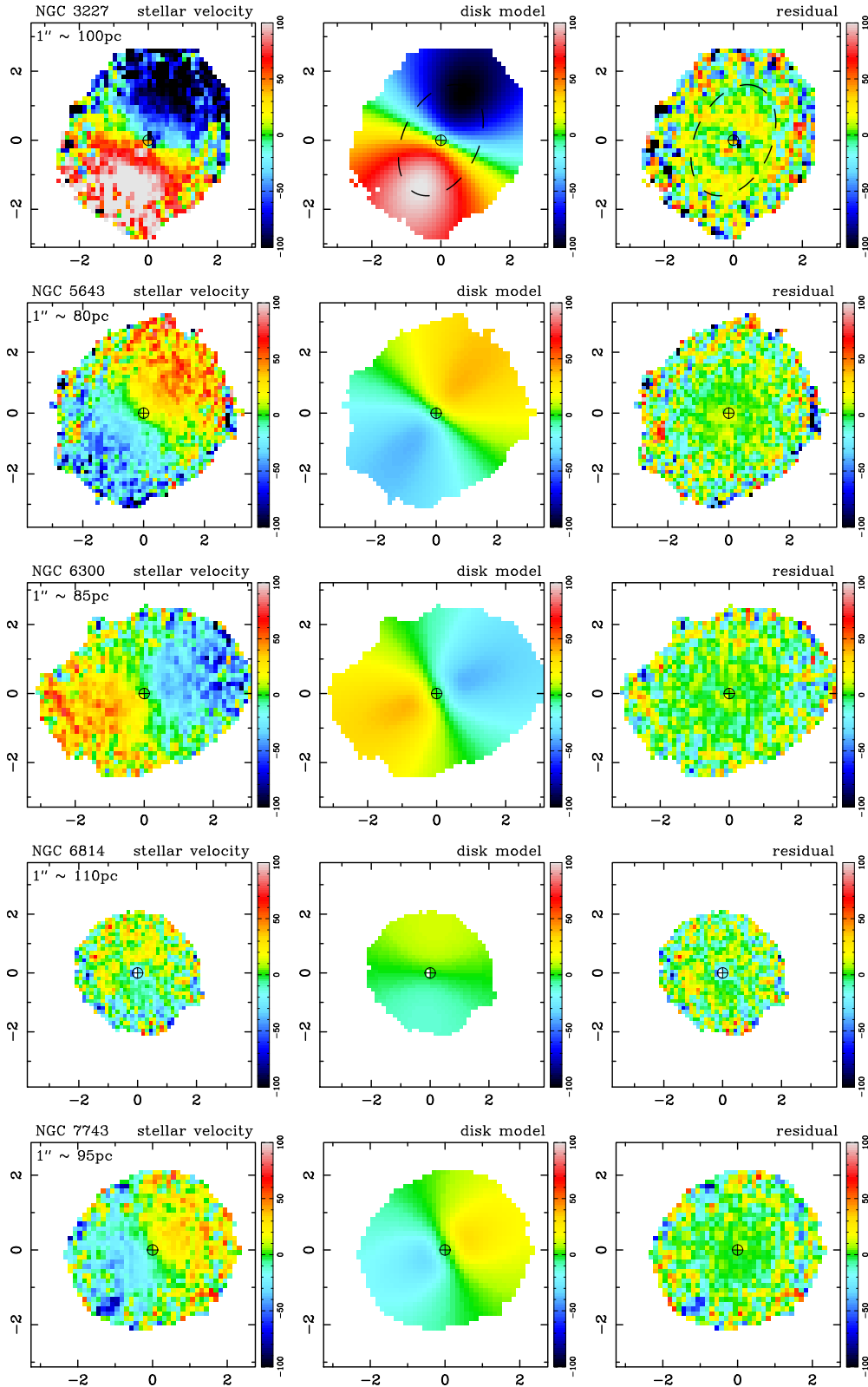


Figure 2. Stellar velocity fields of the active galaxies, together with the very simple disk models and residuals (all plotted on the same velocity scale from -100 to $+100$ km s^{-1}). The model used a rotation curve defined solely by a mass distribution described by a single Sérsic function (with the exception of NGC 7743 for which we included an additional unresolved central mass). The aims were to confirm the orientation adopted for each galaxy, assess whether the stellar velocity fields can be well matched in this way, and hence whether we can apply this method to the more complex H_2 velocity fields in order to determine the non-circular motions of the molecular gas. The dashed ellipse in NGC 3227 traces the circumnuclear ring (Schinnerer et al. 2000; Davies et al. 2006). Axis scales are in arcsec, with a conversion to parsec given for each object; north is up and east is left.

(A color version of this figure is available in the online journal.)

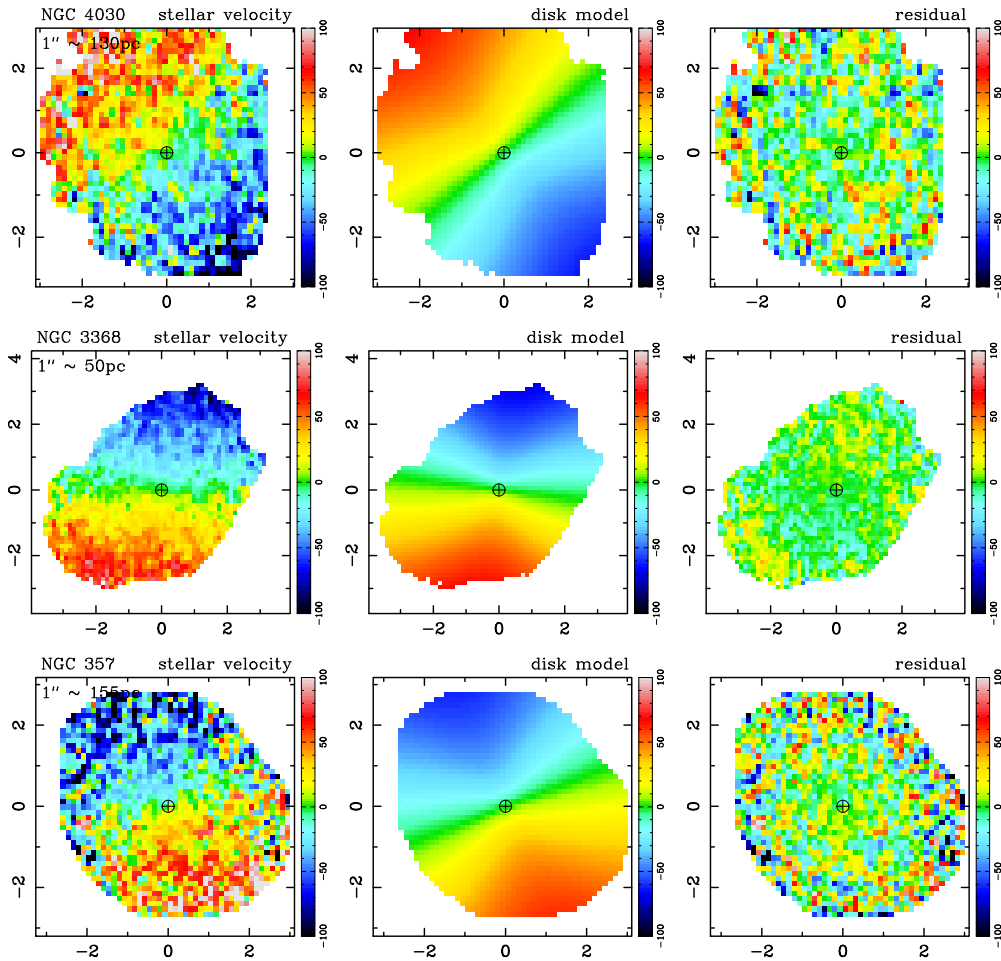


Figure 3. Stellar velocity fields of the three inactive galaxies with measurable velocity gradients, together with simple disk models and residuals (plotted on the same velocity scale from -100 to $+100$ km s^{-1}) as for Figure 2. The two inactive galaxies (IC 5267 and NGC 628) for which no velocity gradient could be measured, and hence for which we do not model the stellar kinematics, are not shown here; their velocity fields are presented in Paper I.

(A color version of this figure is available in the online journal.)

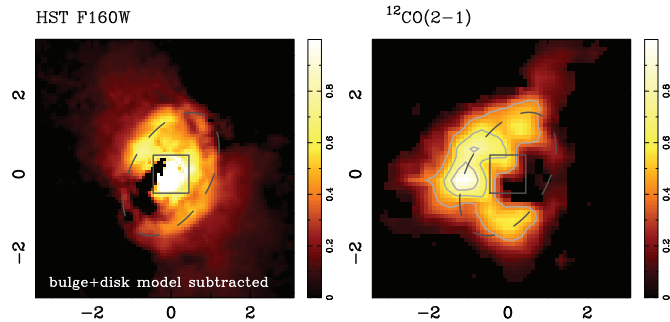


Figure 4. Images of the circumnuclear ring in NGC 3227. Left: H band from HST (square-root scaling), after subtracting a model of the bulge and disk derived from larger scales. Right: the CO 2-1 map from Schinnerer et al. (2000). Reproduced from Davies et al. (2006). The central rectangle indicates the $\sim 1''$ field of view analyzed in that paper, which is significantly smaller than the $6''.5$ field we use here. In this and other figures of NGC 3227, the dashed ellipse represents the location of the circumnuclear ring. Axis scales are in arcsec; north is up and east is left.

(A color version of this figure is available in the online journal.)

$0''.5$ southeast of the nucleus. The elongation of the 1-0 S(1) flux distribution observed in our data is consistent with that in higher resolution data for the same line transition shown in Davies et al. (2006), who presented a detailed view of molecular and ionized gas and their kinematics in the central arcsecond of NGC 3227.

The strongest positive residual that we observe in the H_2 1-0 S(1) emission is located inside the molecular ring reported by Schinnerer et al. (2000), and it is offset from the region of brightest CO 2-1 emission. This suggests that local excitation rather than just the presence of massive molecular clouds plays a role in the excess 1-0 S(1) line flux. However, large amounts of dense molecular gas traced by the HCN(1-0) transition are reported inside the nuclear ring, in the nucleus itself (Schinnerer et al. 2000; Sani et al. 2012; Davies et al. 2012).

The H_2 exhibits a very strong velocity gradient at a P.A. consistent with that of the stars. However, the zero-velocity line (ZVL) shows a remarkable twist: in the innermost $2''$ – $3''$ it is almost straight at P.A. $\sim 40^\circ$, corresponding to the line of nodes (LON) along a P.A. of 130° , slightly discrepant with the stellar LON along a P.A. of 155° . Farther out, the ZVL takes a sharp turn on both sides of the galaxy center, assuming a P.A. of 120° , almost perpendicular to its run in the central parts. For this reason, if we subtract the disk model derived from stellar kinematics, then the largest residuals, with amplitude reaching 100 km s^{-1} , are toward the edges of our field toward both east and west: at radii beyond $2''$ from the nucleus, roughly along the minor axis of the galaxy. Interestingly, at the same locations, the velocity dispersion also increases to ~ 100 km s^{-1} .

High velocity dispersion and high velocity residuals occurring at the outskirts of the field can be caused by outflow

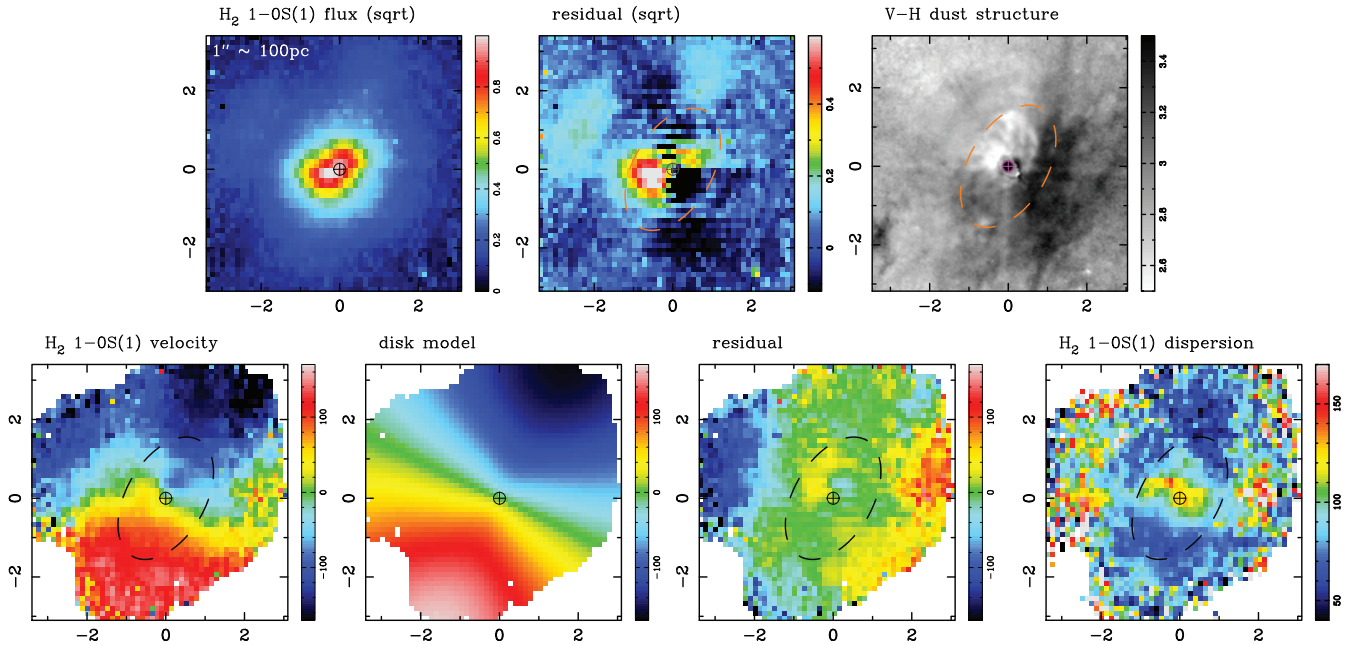


Figure 5. Molecular gas as traced by the 1-0 S(1) line in NGC 3227, showing the same region as in Figure 2. Top row: observed flux, and the residual after subtracting elliptical isophotes centered on the nucleus; the right panel shows the $V-H$ dust structure map reproduced from Martini et al. (2003). Bottom row: observed velocity field, disk model, and the difference between them. The strong residuals a few arcsec from the center suggest that a simple disk is not an appropriate model for this galaxy. The rightmost panel is a map of the velocity dispersion. Axis scales are in arcsec, with a conversion to parsec given; north is up and east is left.

(A color version of this figure is available in the online journal.)

superimposed on rotation there. On the northeast side, these residuals are cospatial with the H_2 flux residual about $3''$ from the center, which may trace the outflowing material. This material is also seen in $H\alpha$ emission in the F658N *HST* filter, with a blueshifted velocity consistent with our measurement (Fischer et al. 2013). In another tracer, the [S III] line at $0.907 \mu\text{m}$, Barbosa et al. (2009) found a NE–SW velocity gradient, with the blueshifted material toward NE extending to $3''$ from the center, at a P.A. somewhat smaller than that of the $H\alpha$ emission and the H_2 residual. They interpreted it as an interaction of the outflowing ejecta with the circumnuclear gas. In the three-dimensional (3D) geometry of the outflow in NGC 3227 proposed by Fischer et al. (2013), the [S III], $H\alpha$ and H_2 emission can all highlight portions of the biconical outflow that intersects the disk plane. This outflow would then be also consistent with the central $2''$ long, high-velocity-dispersion feature in our H_2 data that is extended N–W. However, on small scales, in the adaptive optics integral field spectroscopic data presented by Davies et al. (2006), residual (non-circular) velocities within 50 pc of the nucleus are redshifted at a P.A. around 45° , though the 1-0 S(1) flux is low there. This could be consistent with the locations where the modeled bicone encloses part of the galaxy disk, with the redshift instead of blueshift occurring because we see the other half of the bicone in the high-resolution data of Davies et al. (2006).

To summarize, we see signatures of outflow in the innermost $1-2''$ of NGC 3227, and also in the outskirts of our field. However, at the location of the bend in the ZVL, these signatures are absent. In particular, on the NE side, the H_2 residual emission and the $H\alpha$ emission are weak at the bend of the ZVL, and the velocity dispersion there reaches a local minimum, which counter-indicates multiple components. High velocity dispersion, as well as $H\alpha$ emission and H_2 excess are all located farther out than the bend in the ZVL. This leads us to believe that this bend is not caused by outflow superimposed on the rotation

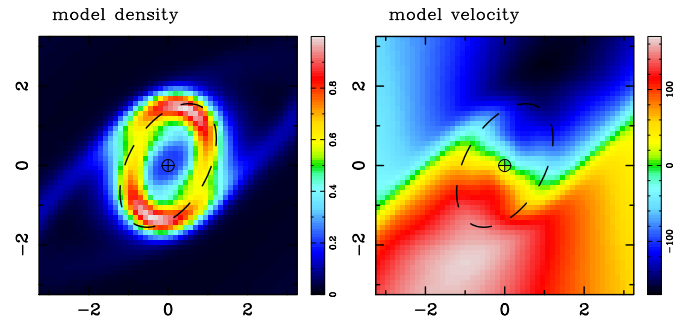


Figure 6. Density (left) and line-of-sight velocity (right) for a hydrodynamical simulation of a disk with a circumnuclear ring (spiral) generated by a large-scale bar, matching model S20 from Maciejewski (2004). The bar was oriented 20° west of the line of nodes, and the model has been set at an inclination and position angle matching NGC 3227 as given in Tables 3 and 4.

(A color version of this figure is available in the online journal.)

in the disk but by gas flow in the disk departing from circular rotation. We noted earlier in this section that NGC 3227 is likely barred, with gas lanes stretching throughout the bar down to the innermost $3''$, where the molecular nuclear ring is present. Hydrodynamical models of gas flow in a bar predict strong inflow in gas lanes that settles on the nuclear ring. Thus strong non-circular motion is expected outside the ring, while in the ring the motion is expected to be close to circular. In Figure 6, we show the LOS velocity for model S20 from Maciejewski (2004) of gas flow in a bar, for the orientation of NGC 3227 given in Tables 3 and 4. There is good qualitative agreement with the velocity field that we observe in NGC 3227 (both the 1-0 S(1) H_2 line in Figure 5 and, within the more restricted region over which it is detected, the $\text{Br}\gamma$ line in Figure 7), with the ZVL bending at the outer parts of the nuclear ring, with blueshift dominating to the east, and redshift to the west. Thus the observed velocity field indicates strong inflow in the bar that settles in the nuclear ring.

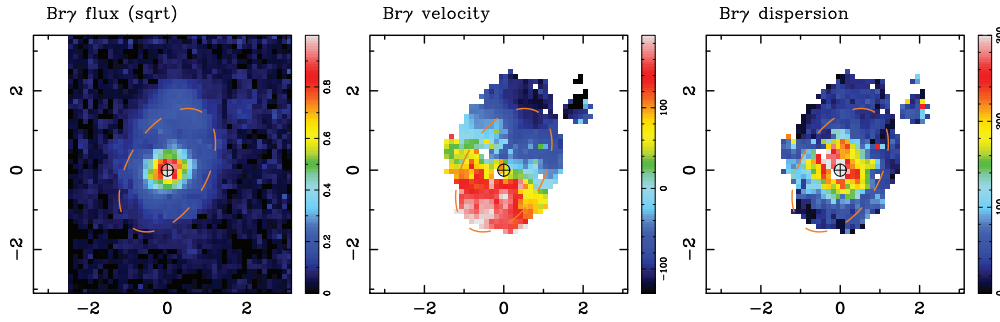


Figure 7. Ionized gas as traced by the narrow Bry line in NGC 3227, over the same field of view as shown previously. The region of high dispersion at the center should be interpreted cautiously, since in this region it was not possible to robustly separate the broad and narrow components. The orange ellipse traces the stellar ring as for Figure 4. Axis scales are in arcsec; north is up and east is left.

(A color version of this figure is available in the online journal.)

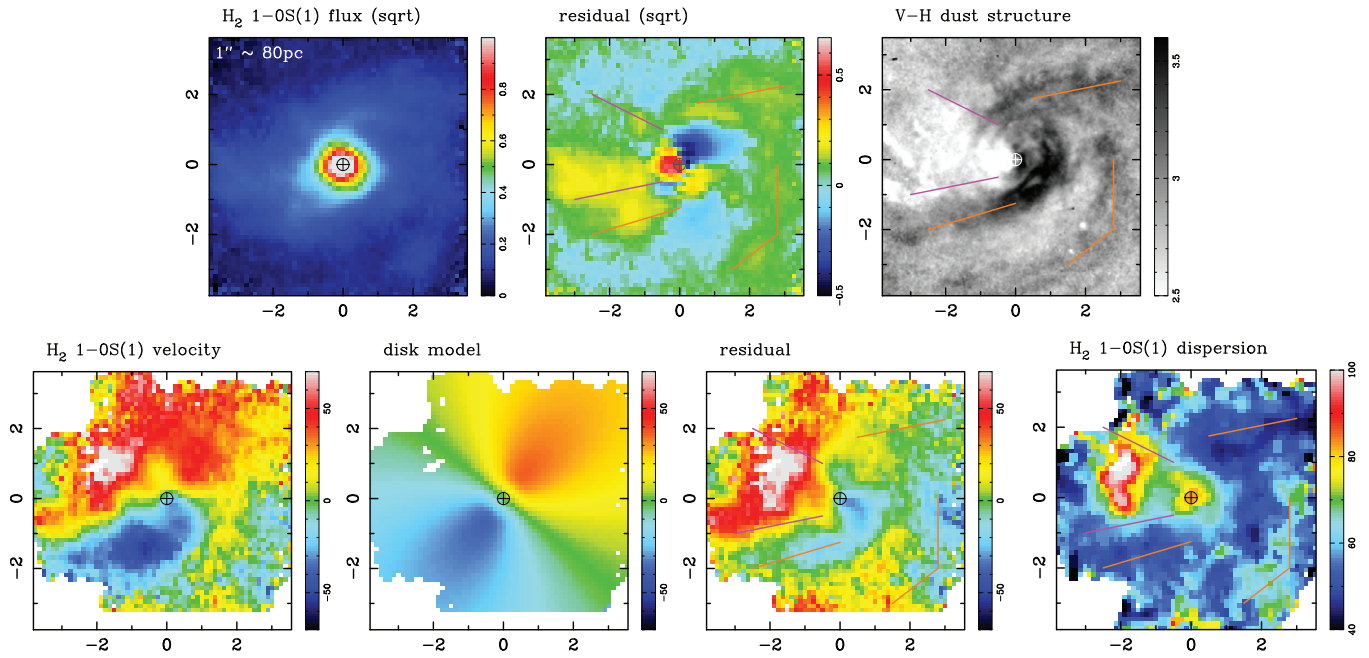


Figure 8. Molecular gas as traced by the 1-0 S(1) line in NGC 5643, showing the same region as in Figure 2. Top row: observed flux distribution, and the residual flux after subtracting elliptical isophotes centered on the nucleus; the right panel shows the $V-H$ dust structure map reproduced from Martini et al. (2003). Bottom row: observed velocity field, disk model, and the difference between them showing the strong velocity residuals in the central few arcsec. The rightmost panel is a map of the velocity dispersion. Magenta lines denote the extent of the eastern outflow as measured from the 1-0 S(1) dispersion and residual velocity maps; these also trace the outline of the low extinction region in the dust structure map. The orange lines trace the three main absorption features in the dust structure map, although we note that the feature to the southwest may in fact be associated with (opposite) outflow rather than inflow. Axis scales are in arcsec, with a conversion to parsec given; north is up and east is left.

(A color version of this figure is available in the online journal.)

NGC 5643

The H_2 1-0 S(1) distribution and kinematics are rather complex in this object. Because much of the FOV is dominated by non-circular motions, a disk model is hard to fit, and to do so, the P.A. needs to be fixed beforehand. As such, when subtracting the best-fitting disk model, the kinematic structure is qualitatively little different from the direct velocity map. On the other hand, the morphological structures do become much clearer when elliptical isophotes are subtracted from the flux map.

Figure 8 confirms that NGC 5643 has a two-arm spiral which is clearly seen in both the dust structure map and the H_2 distribution. In these regions only, the kinematics can be modeled by rotation with modest residuals. As for NGC 3227, in Figure 9, we show for model S20 from Maciejewski (2004) the LOS velocity of gas flow in a bar for a geometry appropriate

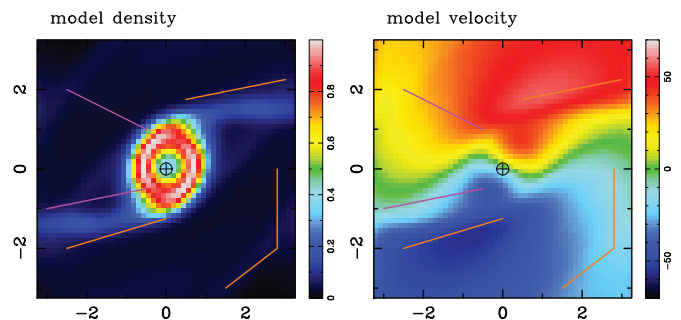


Figure 9. Density (left) and line-of-sight velocity (right) for a hydrodynamical simulation of a disk with a circumnuclear ring (spiral) generated by a large-scale bar, matching model S20 from Maciejewski (2004). The bar was oriented 60° from the line of nodes in the disk plane, and the model has been set at an inclination matching NGC 5643 as given in Table 4, but at a P.A. of -30° , 10° different from that in Table 3.

(A color version of this figure is available in the online journal.)

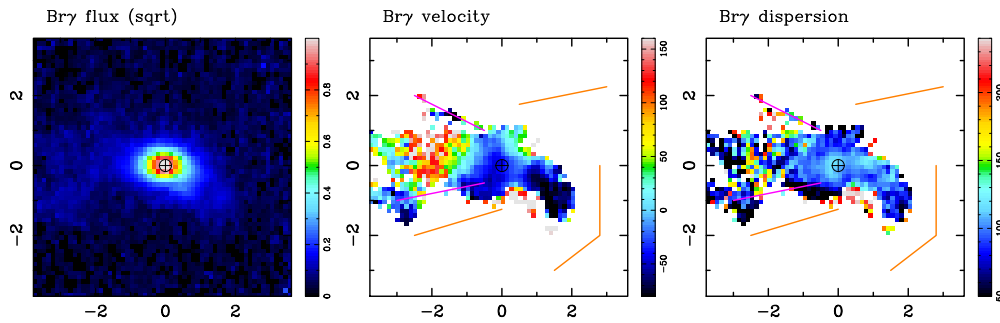


Figure 10. Ionized gas as traced by the $\text{Br}\gamma$ line in NGC 5643, showing the same region as shown previously. Magenta and orange lines are as for Figure 8. Axis scales are in arcsec; north is up and east is left.

(A color version of this figure is available in the online journal.)

to NGC 5643. There is reasonable qualitative agreement with the observed velocity field, and also with the dust and molecular spiral structure.

About $2''$ to the northeast of the nucleus, the kinematics are highly anomalous, with a redshift of 80 km s^{-1} and the dispersion reaching 100 km s^{-1} . At the same location, the dust structure map shows a lighter color in a conical shape toward the east. This indicates less dust, consistent with the reduced 1-0 S(1) flux at the same location, suggesting there is little molecular gas in this region. The simplest interpretation is in terms of outflowing molecular gas excited around the edge of an ionization cone, for which a sketch of the geometry is given in Figure 22 of Fischer et al. (2013). Such a structure extending up to $8''$ to the east is already known from the $\text{H}\alpha$ and [O III] emission lines (Simpson et al. 1997), as well as X-ray imaging at energies $< 3 \text{ keV}$ (Bianchi et al. 2006). The $\text{Br}\gamma$ map in Figure 10 also traces this ionization cone, with velocities exceeding 150 km s^{-1} —somewhat faster than the molecular gas. Based on the [O III] image, and using $\text{H}\alpha$ and [O III] kinematics extracted from a single $0''.2$ wide slit at a P.A. of -128° , Fischer et al. (2013) found that the eastern ionization cone had an opening half-angle of $35\text{--}40^\circ$, and was oriented 65° away from the line of sight but only 42° away from the disk plane. As such, it bisects the disk plane. With this geometry, the emission in the 1-0 S(1) line must trace the far side of the eastern ionization cone, and plausibly originates from ambient molecular gas that was in the disk plane and has been swept up and pushed aside by the outflow.

NGC 5643 has a third molecular structure to the west of the nucleus, extending for approximately $5''$ at a distance of $3''$ west and south of the nucleus. This structure can be seen as a faint arm in the dust structure map. Its presence could be attributed to a transient third arm, the structures of which have been seen in high-resolution simulations of the circumnuclear region (E. Emsellem et al., in preparation). However, it is associated with a higher dispersion than the two arms comprising the grand design circumnuclear spiral. As such, its presence suggests either that the central few hundred parsecs of this galaxy have recently been perturbed, or it could be tracing the far side of the outflow seen more prominently to the northeast. Given that the geometry of the ionization cone suggests it is bisecting the disk, and that the $\text{Br}\gamma$ emission is extended in this direction opposite to the eastern outflow, interpreting the feature in terms of the second ionization cone is appealing. Based on the model of Fischer et al. (2013) one would expect to see the near side of the backward-pointing cone, with moderate blueshifted velocities out to a distance of a few arcseconds. The $\text{Br}\gamma$ emission is consistent with this. H_2 1-0 S(1) could again trace

ambient gas in the disk that is being swept up and heated by the outflow.

NGC 6300

As for most of the other AGNs in our sample, NGC 6300 exhibits complex 1-0 S(1) distribution and kinematics. In this case, we argue that the simplest interpretation is an edge-on outflow superimposed on a rotating disk, although we have detected at best only very weak $\text{Br}\gamma$ emission within the same features.

The residual flux map in Figure 11 reveals a distinct biconical feature, aligned roughly north–south. The flux is enhanced along the limbs of this structure, especially to the south side. On several of the panels in the figures, we have drawn a cross corresponding to it, which enables a better comparison of the locations of features among the various maps. The velocity field shows a strong gradient, which is oriented similarly to that of the stars on the same spatial scales (shown in Figure 2), as well as the large-scale $\text{H}\alpha$ (Buta et al. 2001) and H I (Ryder et al. 1996): clear evidence for a circumnuclear molecular disk. When subtracting a disk model, for which the P.A. was fixed to match that of the stars, the structures in the residual velocity field show a clear blueshift to the north and redshift to the south, following the arms of the cross. A global gradient in the residual can be an indication that the P.A. of the disk model was incorrect. However, when allowing this to vary freely during the fitting process, the structures and their respective velocities remain (although the scale of the residuals is reduced by a factor of two). This suggests that they are real physical features, with a scale of $60\text{--}80 \text{ km s}^{-1}$. Outside the arms of the cross, as well as between them, the residuals are much smaller. A similar X-structure is apparent in the 1-0 S(1) velocity dispersion map, which shows significantly higher dispersion around 100 km s^{-1} along its arms compared to only 50 km s^{-1} between and around them. The simplest interpretation that can simultaneously explain the flux and velocity residuals, as well as the dispersion map, is that they trace the edge of a biconical molecular outflow oriented roughly north–south and seen close to edge-on, with the northern side tilted slightly toward us. The edges of the bicone are brighter because the column of hot gas along those lines of sight is greater, and the dispersion is higher in the same locations because of the range of velocities the gas is tracing. For NGC 6300 we conclude that there is a circumnuclear molecular disk, but we cannot say whether there is inflow because the non-circular velocities are dominated by signatures of outflow.

In contrast to the other AGNs with outflows in our sample, there does not appear to be any extreme reduction in the dust content in the outflow. Nevertheless, the $V-H$ dust structure

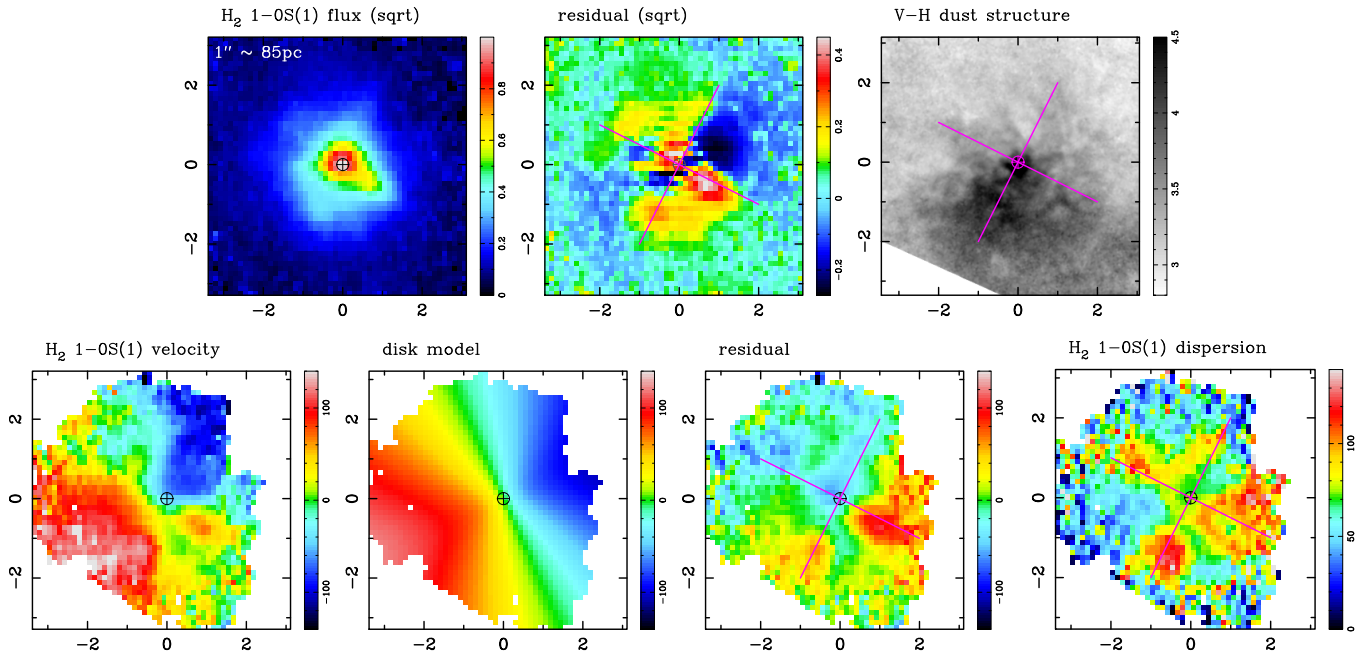


Figure 11. Molecular gas as traced by the 1-0 S(1) line in NGC 6300, showing the same region as in Figure 2. Top row: observed flux distribution, and the residual flux after subtracting elliptical isophotes centered on the nucleus; the right panel shows the $V-H$ dust structure map reproduced from Martini et al. (2003). Bottom row: observed velocity field, disk model, and the difference between them showing the strong velocity residuals in the central few arcsec. The rightmost panel is a map of the velocity dispersion. The crossed magenta lines outline the prominent biconical feature seen in the flux residuals, which also trace regions with the highest velocity residual, and also follow approximately the unusual X-shape in the dispersion map. We note that only a very compact region ($0''.6$ FWHM) of $\text{Br}\gamma$ emission was detected for this object, showing a velocity gradient along the same axis as the 1-0 S(1) line. Axis scales are in arcsec, with a conversion to parsec given; north is up and east is left.

(A color version of this figure is available in the online journal.)

map does show that the northern side is associated with some reduction in obscuration, suggesting that the outflow is in front of the galaxy, consistent with its blueshifted residual velocity.

Our interpretation is consistent with the classification of the [O III] emission by Fischer et al. (2013) as compact because their slit was oriented at P.A. = 90° , roughly perpendicular to the projected axis of the outflow. We note finally that if the gas kinematics in the center of the galaxy are dominated by outflow rather than rotation, this might explain why the line-of-sight velocity of ionized gas in the nucleus differs from the galaxy’s systemic velocity by 100 km s^{-1} (Buta et al. 2001).

NGC 6814

In contrast to the other AGNs in this sample that have extended structures, the H_2 flux in NGC 6814 is rather compact, as can be seen in Figure 12. The adaptive optics data analyzed by Hicks et al. (2009) and Müller-Sánchez et al. (2011) show that the intensity falls to half within a radius of $0''.25$. The gradient in the velocity field presented by these authors—from southeast to northwest—is matched by the seeing-limited data presented here. Müller-Sánchez et al. (2011) analyzed the seeing-limited $\text{Br}\gamma$ and [Si VI] maps extracted from the same datacube, modeling their velocity fields in terms of a rotating disk with a velocity gradient oriented at -35° and a biconical outflow aligned toward a P.A. of $+34^\circ$. While the P.A. of the disk in this model appears different from that of the stellar kinematics on the same scales, discussed in Section 4, the small inclination of the galaxy means that the P.A. has a large uncertainty. Similarly, while longslit spectroscopy on larger scales (Marquez et al. 2004) suggests that the steeper velocity gradient is at a P.A. of 30° rather than -30° , the difference is

much less clear—possibly even reversed—on smaller scales. A slight warp of the nearly face-on disk could easily account for this change. Neither the available H I (Ho et al. 2008) or CO 1-0 data (Curran et al. 2001) are able to shed further light on this because of insufficient spatial resolution.

The 1-0 S(1) velocity gradient is consistent with the -35° P.A. of the disk component modeled by Müller-Sánchez et al. (2011), but also with our adopted -6° P.A. which was used to fit the stellar kinematics. Due to the low flux levels beyond the central compact emission region, the data can be fit equally well with a rotating disk at either of these P.A.s. As such, we cannot draw any conclusion about whether there are indications of molecular inflow or outflow.

NGC 7743

The detailed structures in the 1-0 S(1) flux map become clearer once elliptical isophotes have been subtracted. As Figure 13 shows, this has some resemblance to the $V-H$ dust structure map from which Martini et al. (2003) classified the circumnuclear region of NGC 7743 as a loosely wound spiral. Two arm-like structures, one curving toward the northwest and the other curving round to the south, are apparent in both images. The only feature not traced by the H_2 emission is the arm that continues almost straight out to the southeast. Outside this spiral structure, Moiseev et al. (2004) report two dust lanes in the bar of NGC 7743.

The velocity field also has significant structure and is dominated by non-circular motions. Two spiral arms (one blue and one red) can be traced in the velocity field: the blue arm winds from about P.A. $\sim 0^\circ$ at small radii to P.A. $\sim 180^\circ$ at the outskirts of the FOV, while the red arm is not so well-defined. Such a structure should accompany a density wave of a two-arm

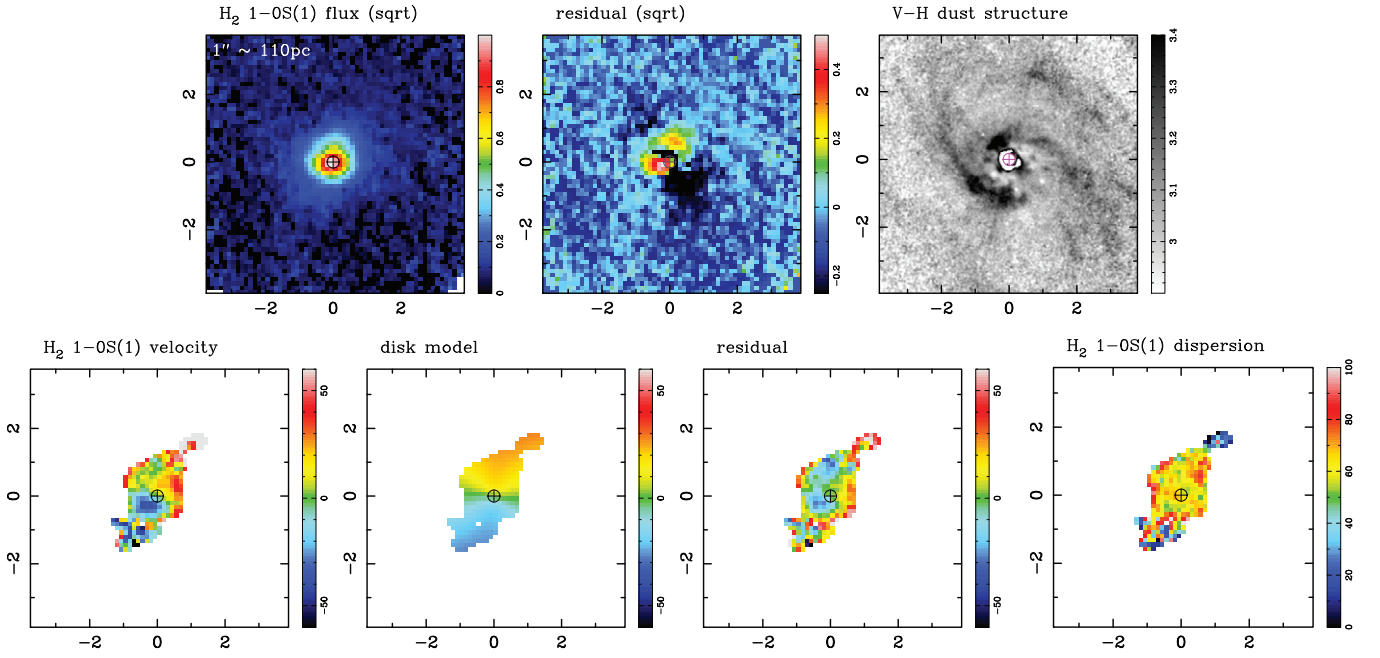


Figure 12. Molecular gas as traced by the 1-0 S(1) line in NGC 6814, showing the same region as in Figure 2. Top row: observed flux distribution and the residual flux after subtracting elliptical isophotes centered on the nucleus; the right panel shows the $V-H$ dust structure map reproduced from Martini et al. (2003). Bottom row: observed velocity field, disk model, and the difference between them showing the strong velocity residuals in the central few arcsec. The rightmost panel is a map of the velocity dispersion. We note that for this object the Br γ flux extracted from the same datacube has already been presented and analyzed by Müller-Sánchez et al. (2011). Axis scales are in arcsec, with a conversion to parsec given; north is up and east is left.

(A color version of this figure is available in the online journal.)

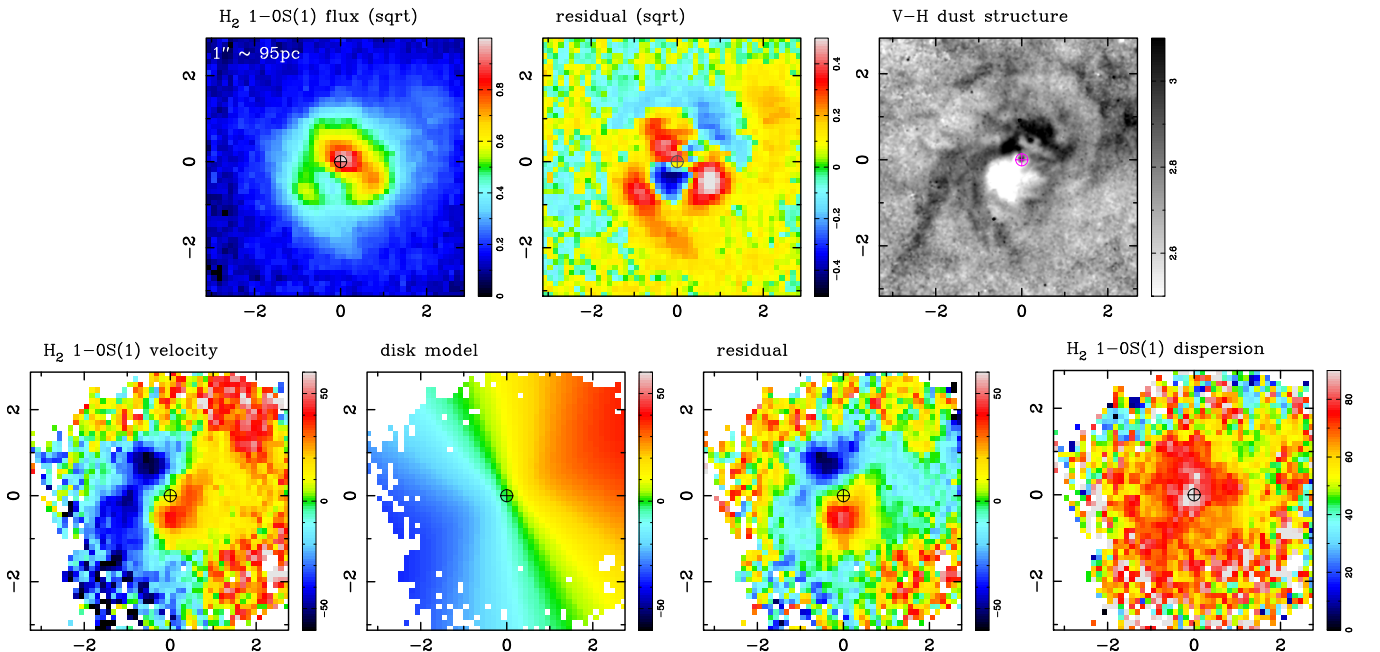


Figure 13. Molecular gas traced by the 1-0 S(1) line in NGC 7743, showing the same region as in Figure 2. Top row: observed flux distribution, and the residual flux after subtracting elliptical isophotes centered on the nucleus; the right panel shows the $V-H$ dust structure map reproduced from Martini et al. (2003). Bottom row: observed velocity field, disk model, and the difference between them showing the strong velocity residuals within an arcsec of the nucleus. The rightmost panel is a map of the velocity dispersion. The red- and blueshifted velocity residuals lie along the minor axis, and neither are spatially coincident with excess 1-0 S(1) flux. In contrast, the redshifted residual is associated with a “hole” in the 1-0 S(1) flux map. The Br γ map for this object shows only very weak emission located within an arcsec north of the nucleus. Axis scales are in arcsec, with a conversion to parsec given; north is up and east is left.

(A color version of this figure is available in the online journal.)

morphology (e.g., Davies et al. 2009), and it is consistent with inflow driven by a circumnuclear spiral, often present inside the straight shocks in the bar and driven by the bar (e.g., Maciejewski 2002, 2004).

However, within the inner 1'', the line-of-sight gas velocity along the LON (P.A. = -65°) is almost zero, which indicates that the tangential velocity of the gas there is almost zero. Thus the velocity field at that location is dominated by a

radial flow (because gas with zero tangential velocity has no angular momentum). This is inconsistent with gas flow in a bar or in a nuclear spiral, where the radial velocity component occurs in addition to the always significant tangential velocity. Moreover, within the inner $1''$ residual velocities no longer form the classical one-arm spiral structure expected for a two-arm photometric spiral (e.g., Maciejewski 2004; Davies et al. 2009; Schnorr-Müller et al. 2014), but are instead consistent with a signature of radial flow. Thus, while at radii $\gtrsim 1''$ the dust structure and the gas kinematics are consistent with inflow in a nuclear spiral, the gradient of the line-of-sight velocity between $+50$ to -50 km s^{-1} within $\sim 1''$ of the nucleus along the minor axis is most likely caused by a radial flow.

This radial flow can either be isotropic in the plane of the galaxy disk, or can be out of the disk plane. In order to assess whether this is due to inflow or outflow, we must consider which are the near and far sides of the galaxy. In optical images of the galaxy, the spiral arms on large scales in the disk wind, from the center outward, in an anti-clockwise direction on sky (Moiseev et al. 2004). The circumnuclear spiral structure is wound in the same sense. Since the velocity field implies the approaching side is to the east, for the spiral arms to be trailing, the north side of the galaxy must be the near side. Thus, we can state that, if the redshifted residual to the south and the blueshifted residual to the north arise from material in the disk plane, then this material must be flowing outward.

That these features trace outflowing gas is also true if the material is in front of the disk to the north, and behind the disk to the south, or if it is in a feature inclined to the galaxy disk by less than 37° (the inclination of NGC 7743) in such a way that the blueshifted feature is behind the galaxy disk and the redshifted feature is in front of it. This is consistent with the interpretation of the feature present in the residual velocity field in terms of an AGN-driven outflow.

An outflow would be consistent with the high dispersion of $\sim 70 \text{ km s}^{-1}$ in these regions. But perhaps stronger support for this interpretation comes from the $[\text{O III}]$ line, which is typically taken to be excited by an AGN and trace its ionization cone. In NGC 7743, $[\text{O III}]$ emission is extended along the minor axis and shows a markedly different velocity gradient from the stars (Moiseev et al. 2004; Katkov et al. 2011). Indeed, to the north side at a P.A. of 358° , the $[\text{O III}]$ line is blueshifted, while to the south it is redshifted with respect to the stars (see Figure 13 of Moiseev et al. 2004 and top right panel of Figure 2 in Katkov et al. 2011). While the $\text{H}\beta$ kinematics follow the stars on scales $> 10''$, at $< 5''$ they instead match those of $[\text{O III}]$. Remarkably, Katkov et al. (2011) also note that the highest dispersion in the $[\text{O III}]$ line is $1\text{--}2''$ south of the nucleus. Using their high spectral resolution spectra, they show that here the line is comprised of two components, one of which is blueshifted by 300 km s^{-1} with respect to the primary component. The spatial location of this component coincides with the location of the white region in the dust structure map, which shows there is almost no dust. As is apparent for the other AGNs in our sample, regions of low extinction and low molecular gas content such as this are typically associated with outflows. We note that low extinction in the cone has been observed for other AGNs, e.g., NGC 4945 (Moorwood et al. 1996; Marconi et al. 2000). Putting these facts together in the context of the conical outflow models employed by Fischer et al. (2013), we conclude that to the south of the nucleus, the outflow is in front of the galaxy disk. As illustrated in Figure 14, in this context:

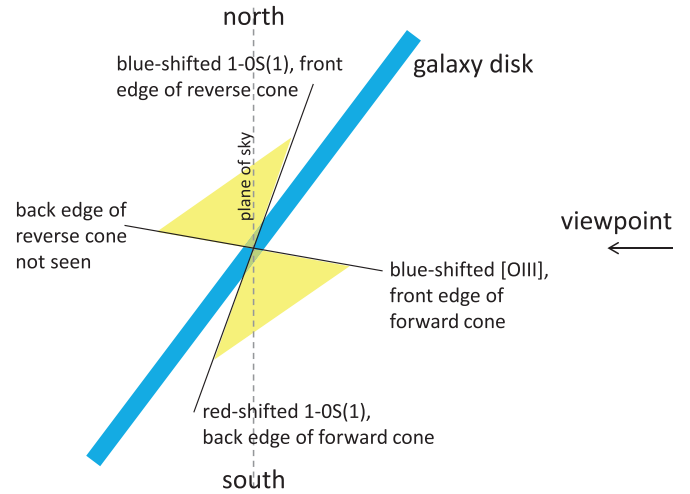


Figure 14. Sketch of our proposed geometry for the outflow in NGC 7743, as described in the text.

(A color version of this figure is available in the online journal.)

1. the blueshifted $[\text{O III}]$ emission close to, but south of, the nucleus traces an edge of the cone that is oriented almost directly toward us but still blocks the direct line-of-sight to the nucleus;
2. the redshifted 1-0 S(1) and $[\text{O III}]$ emission south of the nucleus traces the back edge of the cone which is tilted behind the plane of the sky, but may still be in front of the disk; we see H_2 emission from this edge because it is close to the galaxy disk where there is a supply of ambient molecular gas;
3. the blueshifted $[\text{O III}]$ and 1-0 S(1) emission to the north traces the near side of the opposite (backward-pointing) cone, which lies behind the galaxy disk but is still tilted forward from the plane of the sky;
4. we do not see the counterpart to (i) above because it is obscured behind the central regions of the galaxy.

In this interpretation of the various emission components, the opening half-angle of the cone must be large, probably in the range $40^\circ\text{--}60^\circ$, so that one edge is angled toward us while the other is close to the galaxy disk. We note that the 3D modeling of outflow geometries by Müller-Sánchez et al. (2011) and Fischer et al. (2013) suggests that opening angles this wide may not be untypical. The interpretation is also consistent with the classification of this AGN as a Seyfert 2, for which one should expect an outflow to be tilted away from our line of sight. This then requires the outflow to be strongly tilted with respect to the normal to the disk plane. Such orientations may be common: there is thought to be little or no relation between host and outflow orientation, and Fischer et al. (2013) found a significant number that were tilted by $30^\circ\text{--}50^\circ$ from the normal to the disk.

5.2. Inactive Sample

Three of these objects (NGC 4030, NGC 628, NGC 357) have no 1-0 S(1) line emission detected, so there are only two objects for which we can study the H_2 distribution and kinematics. That both of these show severe disturbances is perhaps unexpected. Inflow of gas from external streamers is the most promising explanation, and only a small perturbation is now required to trigger a major molecular gas inflow event and turn these objects into AGNs.

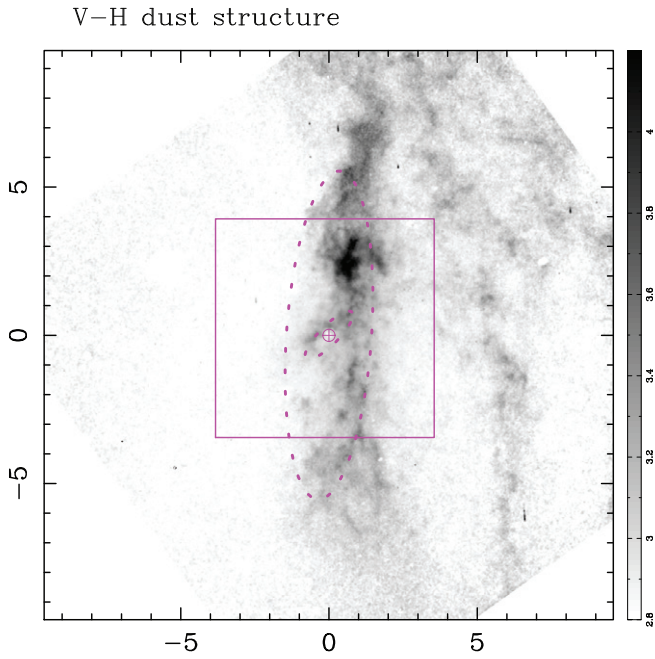


Figure 15. Dust structure ($V-H$) map of IC 5267 reproduced from Martini et al. (2003). The field of view of SINFONI, shown in the corresponding Figure 16, is marked. In addition, the same ellipses as shown in some panels of that figure are overdrawn with dotted lines. Axis scales are in arcsec; north is up and east is left.

(A color version of this figure is available in the online journal.)

IC 5267

The H_2 distribution and kinematics in the central few hundred parsecs, shown in Figure 16, appear totally unrelated to the stars, which exhibit no measurable velocity gradient (Paper 1). On scales of a few arcsec, the warm molecular gas lies in a narrow

north-south band with a strong velocity gradient, spatially coincident with the band of extinction in the dust structure map of Martini et al. (2003), which is reproduced in Figure 15. This band is part of a larger dust structure most likely located in front of the galaxy disk (Mulchaey et al. 1997). The much more intense H_2 emission within $\sim 1''$ of the nucleus comes from another elongated structure, separated from the north-south band by an abrupt change of P.A., and having a velocity gradient with the opposite sense (redshifted gas is toward the south rather than the north). This inner H_2 feature is spatially coincident with a much fainter dust lane that approximately shares its extent and P.A. These kinematics are consistent with a possible moderate ($< 10 \text{ km s}^{-1}$) counter-rotation observed in stars (Morelli et al. 2008) and a stronger (30 km s^{-1}) counter-rotation in ionized gas (L. Morelli 2013, private communication). If the system were close to face-on, the observed kinematics could be caused by a modest warp, so that the disk's outer part is tilted slightly behind the plane of the sky and its inner part slightly in front along the same radial direction (see, e.g., Engel et al. 2010; Diaz & Dottori 2013). However, the narrow dust lane in the north-south direction indicates that at least part of the system is close to edge-on, which is inconsistent with the warp scenario.

The most natural interpretation is that the system consists of at least two separate components: one is the north-south dust lane, together with the associated H_2 emission extending across the full SINFONI field, and the other is the inner H_2 emission of distinctly different kinematics, associated with the weaker dust lane. The increased gas dispersion at the boundary between these two components is then caused by the two components overlapping there. The first component is likely part of a streamer in front of the galaxy. If we assume that this streamer is edge-on and orbiting the galaxy nucleus, we can estimate the maximum radial distance at which it can be in order to yield the observed projected velocity of $\pm 150 \text{ km s}^{-1}$

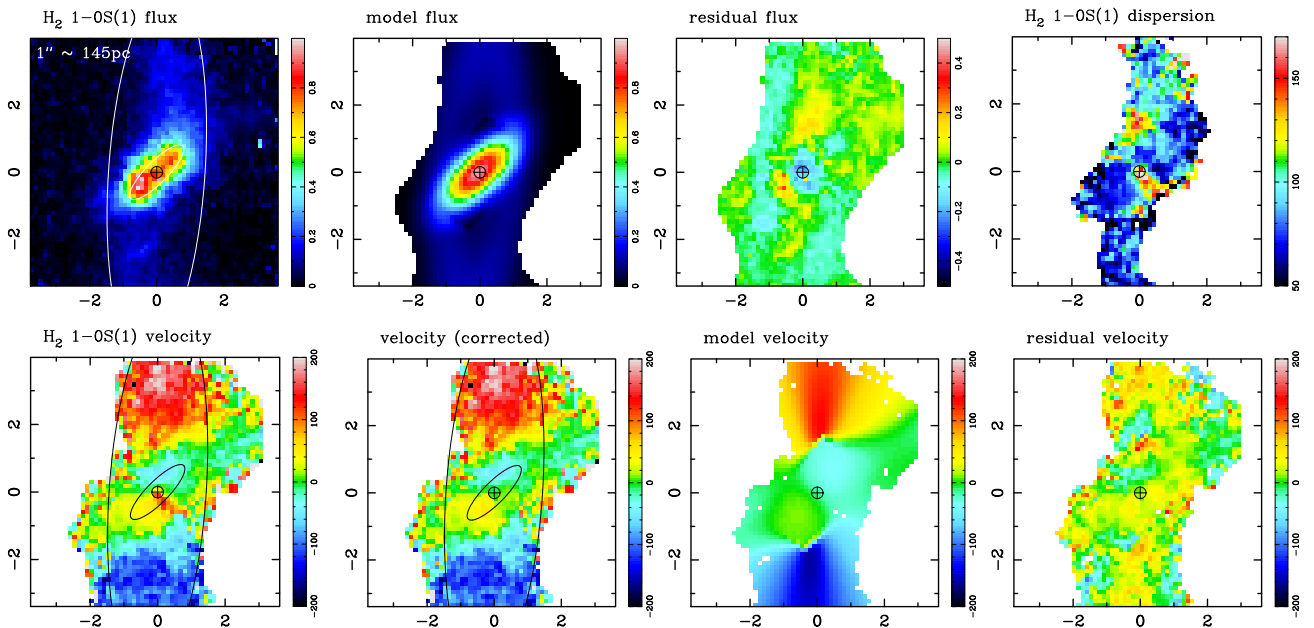


Figure 16. Molecular gas as traced by the 1-0 S(1) line in IC 5267. Top row: observed flux distribution, the model comprised of two rings, and the difference between them (note that some of the differences may be due to the model being axisymmetric while the illumination of the rings may vary between locations). On the far right is shown the velocity dispersion. Bottom row: observed velocity field, before and after correcting for the double peaked line profile causing the finger of anomalous velocities extending southwest from the nucleus (see the text for details). On the right side are the two-ring model, and the residual velocity after subtracting this model. The two ellipses represent the two rings (drawn corresponding to a size of Radius+FWHM/2, as given in Table 5, to denote the full extent of the two structures). Axis scales are in arcsec, with a conversion to parsec given; north is up and east is left.

(A color version of this figure is available in the online journal.)

Table 5
Properties of the Two Rings in IC 5267

Radius (")	FWHM (")	Rel. Int.	P.A. (° E of N)	i (°)	M_{enc} (M_{\odot})	V_{rot} (km s^{-1})	τ_{orb} (Myr)
3.9	3.3	1.0	-4	75	2.5×10^9	139	25
0.2 ^a	1.8	6.2	135	73	3.0×10^7	66	3

Note. ^a Because the fit yields a radius of the ring smaller than its width, this can be considered a disk with a rather flat inner radial profile, extending out to $1''.1$.

at an offset of $\pm 3''$ (440 pc) in projection. Since the H I line profile has a full width of 400 km s^{-1} (van Driel et al. 1988), the maximum rotation velocity is 300 km s^{-1} for an inclination of 42° . The maximum distance of the streamer from the center is then ~ 900 pc. The second component is a disk or a ring that extends radially to about 250 pc, with a P.A. and inclination that are different from the streamer, but closer to those of the galaxy disk on large scales. Such a scenario, with gas orbiting in two different planes, can only be quasi-stable and would not require much to perturb it.

In order to test this interpretation further by attempting to reproduce the observed 1-0 S(1) flux map and velocity field, we model this streamer, and also the more compact structure in the 1-0 S(1) map, as two rings of gas. Using DYSMAL, we have created a model, shown in Figure 16, which is comprised of two massless rings with circular orbits. The best-fitting model was obtained by varying the enclosed mass together with the ring radius, width, P.A., and inclination for both rings in order to obtain the best fit to the flux and velocity maps for all pixels above a given 1-0 S(1) flux threshold (the extent of the mask can be traced in the figure). The parameters of the best fitting model are summarized in Table 5, and indicate that both rings are close to edge-on but nearly counter-rotating, as they differ in P.A. by 140° . In this model, the outer ring is broad, extending from 330 pc to 810 pc. The radius of the inner ring is formally 30 pc, but its large FWHM indicates that it is effectively a disk, whose intensity drops to half of the maximum value at 160 pc, and is also slightly less than the maximum at radii smaller than 30 pc. Thus the inner component has a relatively flat inner luminosity distribution (we have modeled it as a ring rather than an axisymmetric centrally peaked disk only to better match the dip in 1-0 S(1) flux at the center). The enclosed masses are well-defined. The inner ring yields an upper limit (excluding the impact of dispersion) on the mass of a central black hole of $3 \times 10^7 M_{\odot}$. This is more than 1.2 dex below the $M_{\text{BH}}-\sigma$ relation, given the stellar velocity dispersion in the bulge of 200 km s^{-1} (Morelli et al. 2008). The outer ring suggests there is a considerable mass of stars in the central few hundred parsecs. There is a chance for gas clouds to collide where the orbital planes of the two structures intersect. This will occur if either the gas in the rings diffuses inward or outward, or if there is cool gas already distributed through the orbital planes that we cannot trace with the 1-0 S(1) line. If a sufficient mass of gas begins then begins to fall inward, the galaxy would become an AGN within a relatively short time given the orbital timescales for both rings.

One obvious discrepancy between the observed and modeled velocity fields is the ZVL of the inner structure: in the data this is at a P.A. of 90° while the model puts it at 45° matching the 135° orientation of the LON. One way to account for this difference is to assume that a radial flow is superimposed on the circular motion. However, matching the observed ZVL and LON

requires outflow at a velocity of 0.3 times the rotation speed. Alternatively, the difference may be the result of gas moving on elliptical orbits (see the Appendix of Mazzalay et al. 2014) instead of being in circular motion in the inner structure. For the observed P.A. of the flux distribution in the inner structure of 135° , the observed axial ratio of the structure of about 0.3, and the P.A. of the ZVL of 90° , only one P.A. of the LON is possible: P.A. = 140° . This is exactly the P.A. of the large-scale galactic disk. The inclination is unconstrained and is tied only to the intrinsic ellipticity of the orbits. If we assume that the inner structure is in the galactic disk, then at $i = 40^\circ$, we get an intrinsic axis ratio $b/a = 0.4$, implying a rather eccentric flow. Moreover, such gas in the inner structure, being in the disk plane, would rotate in the direction opposite to the large-scale H I (van Driel et al. 1988). On the other hand, the elliptical flow is roundest, with $b/a = 0.77$, when the inclination is close to $i = 73^\circ$, which is the inclination of the inner ring in the model above that assumes circular flow.

One final anomaly in the 1-0 S(1) data is the finger of high velocity extending about $1''$ to the southwest from the nucleus. This feature appears also in the dispersion map and is the result of a second peak in the emission line, redshifted by about 200 km s^{-1} with respect to systemic. Separating the two components in the flux and velocity maps (Figure 16, bottom panels) suggests this extra feature is spatially unresolved and centered close to the nucleus. Thus there may be a third component in our data, located within 150 pc of the nucleus (in projection), and moving at 200 km s^{-1} relative to it.

In summary, these two discrepancies (the P.A. of the ZVL and the finger of high dispersion) shed light on the details of the inner disk structure in IC 5267, but do not detract from the interpretation that the molecular gas is confined to two independent planes rotating at different orientations.

NGC 3368

The H_2 distribution is not centered on the nucleus of this galaxy, but peaks about $0''.4$ north, as can be seen in Figure 17. Some fainter structure is also apparent and can be seen more clearly in the second panel of the figure, which shows the residual flux after fitting and subtracting elliptical isophotes. The offset of the brightest H_2 emission was reported by Nowak et al. (2010), and their adaptive optics data resolved it into two knots that appeared to be moving at different, unrelated velocities, decoupled from the disk rotation.

Our larger-scale velocity field also shows structure near the nucleus, although overall it is dominated by rotation with a velocity of 180 km s^{-1} at a radius of $2''$. We see no signature of gas inflow in the bar, despite a double bar being reported in NGC 3368 by Erwin (2004), with the inner bar confined within our SINFONI field (semimajor axis of $4\text{--}5''$) and present in the continuum data. The LON of the stellar and gas velocity field is consistent with the LON determined on larger scales. Fitting and removing the global rotation with a disk model reveals an extended structure remarkably similar to that expected for coherent counter-rotation, centered about $0''.4$ north of the nucleus. This velocity structure can be traced beyond a radius of $1''$ from its center, and as such filled most of the FOV observed by Nowak et al. (2010), which made their H_2 velocity field difficult to interpret. It is also apparent in the velocity map of the 1.3 mm CO 2-1 line, at a similar spatial resolution to our data (Haan et al. 2009), the central part of which is reproduced in Figure 18. This argues against the idea that the H_2 emission is simply two knots moving rapidly in opposite directions with

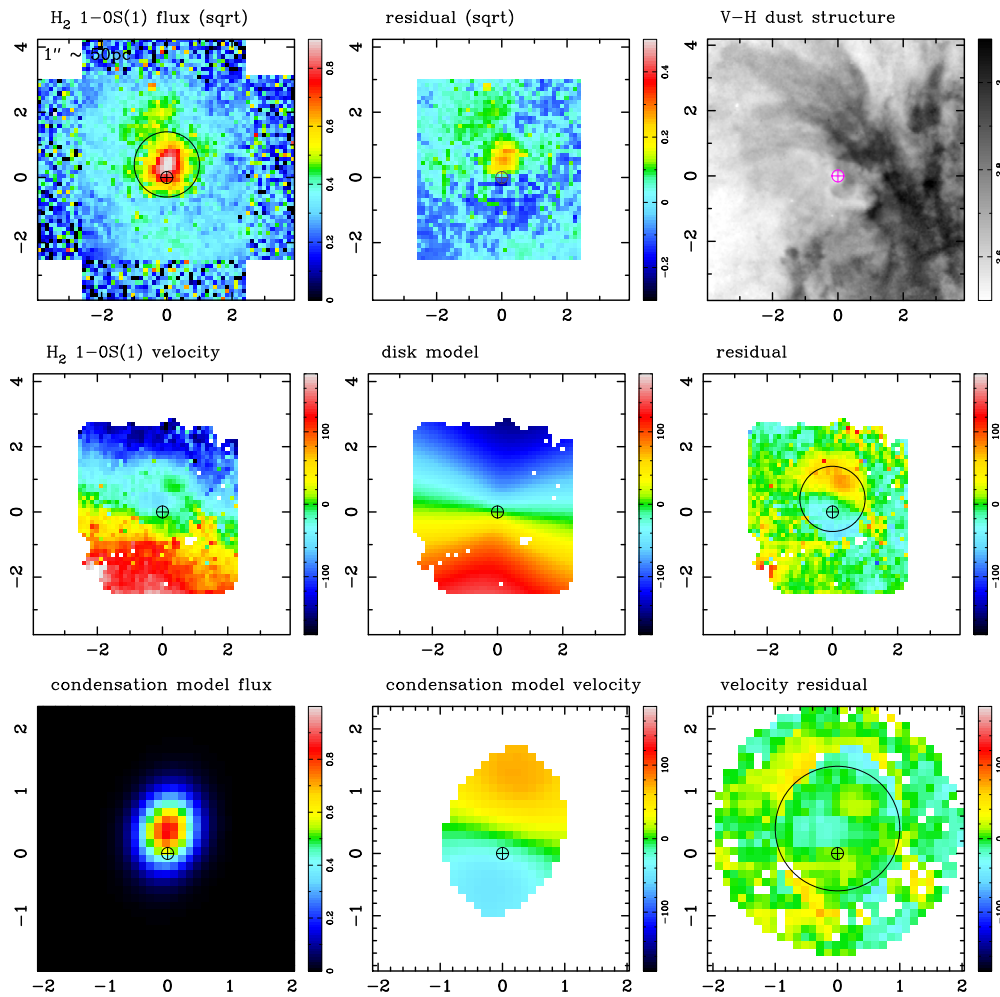


Figure 17. Molecular gas as traced by the 1-0 S(1) line in NGC 3368, showing the same region as in Figures 1 and 3. Top row: observed flux distribution, and the residual flux after subtracting elliptical isophotes centered on the nucleus; the right panel shows the $V-H$ dust structure map reproduced from Martini et al. (2003). Middle row: observed velocity field, disk model, and the difference between them showing the clear counter-rotation centered about $0.4''$ north of the nucleus. Bottom row: zoomed-in view of the flux, velocity, and velocity residual (with respect to the rightmost panel in the middle row) of the counter-rotating condensation model. The circle is centered $0.4''$ north of the nucleus (near the peak of the 1-0 S(1) emission in the top-left panel) and has a radius of $1''$. Although the flux of this off-center knot is compact, the impact of its velocity field can be traced out to $\sim 1.5''$. Axis scales are in arcsec, with a conversion to parsec given; north is up and east is left.

(A color version of this figure is available in the online journal.)

respect to the galaxy disk. Instead, a simple explanation could be that the two knots are bright spots in a self-gravitating molecular condensation (i.e., cloud or cloud complex) that is also traced partly by the CO line emission.

However, it is difficult to reconcile the vastly different distributions of the two molecular gas tracers in this context: the 1-0 S(1) line emission to the north of the nucleus is between the brightest CO 2-1 emitting knots which lie to the northwest and northeast of the nucleus. This must be related to the gas temperature, since the former traces gas at 1000–2000 K while the latter typically traces gas at 10–100 K. Normally, these are expected to trace broadly similar distributions. However, on these scales, where the resolution corresponds to only 30 pc, local heating effects play a major role in the flux distribution (see, for example, the relative distributions of CO 2-1 and 1-0 S(1) in the central 300 pc of NGC 1068, Müller-Sánchez et al. 2009).

In order to pursue the idea of a molecular condensation, and to provide an approximate constraint on its properties, we have modeled it as a thin rotating disk with a mass distribution described by a Sérsic function. We fit the model to the residual 1-0 S(1) velocity field (but not to the flux distribution) as shown

in the bottom panels of Figure 17). While the model can only be representative rather than highly constrained, it suggests that the condensation is slightly inclined, has a rotation velocity of 70 km s^{-1} at a radius of $1''$, and that the mean velocity is offset from that of the disk by more than 10 km s^{-1} . It is possible that such a gas condensation has arisen internally, perhaps similar to the $10^7 M_{\odot}$ star cluster in the circumnuclear region of M83 (Piqueras López et al. 2012), which also exhibits internal rotation unrelated to the host galaxy but without any significant systematic velocity offset. On the other hand, as discussed in Section 3, there is unambiguous evidence from observations of intergalactic H I that there is a bridge of gas leading to NGC 3368 (Michel-Dansac et al. 2010). As such, external accretion of gas is a natural, and simple, explanation for the condensation. Furthermore, because molecular gas moving anomalously in the disk plane would rapidly lose angular momentum, it seems likely that the condensation lies out of the disk plane, and hence may be moving on an orbit unrelated to the disk. If it is in front of the disk plane, then it would be falling toward the disk. Such an orbit, combined with the paucity of gas in the disk, could explain why the condensation has survived long enough to be observed. Although we cannot fully rule out an origin

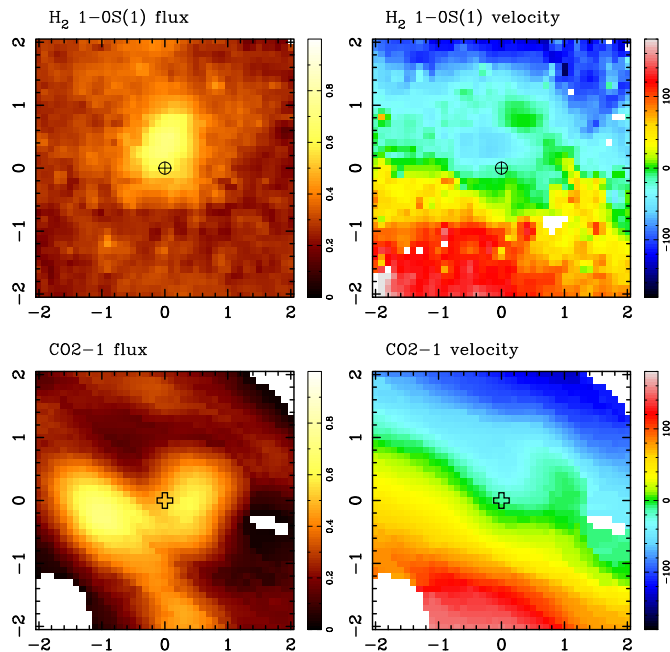


Figure 18. Molecular gas as traced by the 1-0 S(1) and CO 2-1 lines in the central $4'' \times 4''$ of NGC 3368. Top row: flux and velocity of the 1-0 S(1) line. The crossed circle denotes the center as measured from the K -band peak. Bottom row: flux and velocity of the CO 2-1 line. The hollow plus denotes the dynamical center derived by Haan et al. (2009). The flux maps of the two tracers are remarkably different and so we have registered them by assuming that the dynamical center of the CO map is located at the K -band continuum peak. When this is done, the non-circular velocities to the northwest of the nucleus match up between the near-infrared 1-0 S(1) line and the 1.3 mm CO 2-1 line. Axis scales are in arcsec; north is up and east is left.

(A color version of this figure is available in the online journal.)

from secular processes, the anomalous orbit argues rather for accretion of gas from a streamer as its origin.

Ignoring velocity dispersion, the dynamical mass of the structure is $\sim 6 \times 10^7 M_{\odot}$. This estimate is close to the minimum since, even if the modeled disk were edge-on, the dynamical mass would decrease only a little. We have tested the plausibility of this dynamical mass by performing an independent estimate of the gas mass in the two brightest CO 2-1 knots based on their luminosities. Adopting a CO-to- H_2 conversion factor of $\alpha_{CO} = 4.3 M_{\odot} (\text{K km s}^{-1} \text{pc}^2)^{-1}$ (Bolatto et al. 2013) yields a mass in the right and left knots of $6 \times 10^7 M_{\odot}$ and $7 \times 10^7 M_{\odot}$ respectively. These two knots comprise about 40% of the CO luminosity, and hence mass, in the $4''$ field shown in Figure 18, and a little under 20% of the mass in the CO “core” reported by Sakamoto et al. (1999) (once their adopted distance to this object is matched to ours). Thus, both the CO luminosity of the right-hand knot and the dynamical mass derived from the 1-0 S(1) residual velocities are consistent and point to a substantial mass in this condensation. In the Appendix and Figure 1 we showed that there was residual stellar continuum just east of the nucleus. The stellar mass associated with this was in the range $1\text{--}5 \times 10^6 M_{\odot}$. As such, the gas fraction of the condensation is very high, indicating that it should not be considered as a dwarf galaxy, but as associated with the gas streamers.

The mass of the condensation is very significant compared to that in the galaxy at these scales. Taking a stellar velocity dispersion of 120 km s^{-1} (Paper I), one can estimate the dynamical mass of the galaxy within 0.4 of its nucleus as $2 \times 10^8 M_{\odot}$, only a factor 3–4 greater. As such, when the condensation does merge with the galaxy nucleus, it will have a marked impact.

Interestingly, the model of the condensation requires a steep rise in the rotation curve, reaching a maximum of nearly 90 km s^{-1} at a radius of 0.3 . This could account for the high anomalous velocities of the two bright knots of H_2 emission noted by Nowak et al. (2010): they light up the most rapidly moving part of the condensation, perhaps through thermal or shock heating since the shear at this point would be a maximum.

6. RECENT VERSUS ONGOING NUCLEAR STAR FORMATION

To assess the age of the stellar population in the sample of galaxies, we estimate the equivalent width of the $\text{Br}\gamma$ emission. As can be seen in Table 2, within a $2''$ aperture (corresponding to a radius of typically 100 pc) $\text{Br}\gamma$ emission is detected in four of the five active galaxies, the exception being the lowest luminosity Seyfert NGC 7743. No $\text{Br}\gamma$ emission is detected in any of the inactive galaxies. The equivalent width is calculated using the stellar K -band luminosity, which is determined from the total K -band luminosities given in Table 2 corrected for any AGN contribution. The fraction of the K -band luminosity attributable to non-stellar AGN continuum is estimated from the dilution of the CO bandheads, which are expected to have a constant (to within 20%) intrinsic equivalent width over a wide range of star formation histories and ages (Davies et al. 2007). The dilution factor for each galaxy was determined from an integrated spectrum within the same $2''$ aperture and, consistent with our results presented in Paper I, only three of the galaxies have signs of significant AGN contribution to the continuum. These are NGC 3227, NGC 6300, and NGC 6814, which have dilution factors of 0.41, 0.59, and 0.55, respectively. It is this correction factor that is used to determine the stellar K -band luminosity and to calculate the $\text{Br}\gamma$ equivalent width (i.e., $L_{\text{stellar}} = L_K \times f_{\text{dilution}}$). As shown in Table 2, 3σ upper limits on the $\text{Br}\gamma$ luminosities and equivalent widths are also given for those galaxies in which no $\text{Br}\gamma$ emission is detected within the integrated $2''$ aperture spectra.

The low $\text{Br}\gamma$ equivalent widths, ranging from 0.1–1.4 Å (Table 2), suggest that there is no ongoing star formation in our sample on the scales measured. These equivalent width values are characteristic of a stellar population that is at least 10 Myr old and potentially as old as a few 100 Myr, depending on the assumed star formation history (e.g., Davies et al. 2007). Although the measured $\text{Br}\gamma$ equivalent widths rule out ongoing star formation, they do not exclude the possibility of relatively recent star formation within the circumnuclear region measured.

Esquej et al. (2014) find evidence for recent star formation in 45% of their sample of Seyfert galaxies using $11.3 \mu\text{m}$ polycyclic aromatic hydrocarbons (PAHs) emission. They measure the star formation activity in the vicinity of the AGN on scales similar to those probed with our sample, as well as on larger scales of hundreds of parsecs, and find that the activity detected is centrally concentrated to scales of tens of parsecs. In the fraction of the sample in which the PAH emission was not detected there is either no star formation occurring or the population has aged such that B stars have evolved off the main sequence. Although PAH emission is a tracer of young stars, it is believed that the emission is more sensitive to B stars than O stars (Peeters et al. 2004). Díaz-Santos et al. (2010) verify this by showing that the PAH/ $\text{Pa}\alpha$ ratio increases for lower $\text{Pa}\alpha$ equivalent width. Since the equivalent width of $\text{Pa}\alpha$ is an indicator of age this implies that the PAHs trace older stars than the hydrogen recombination lines sensitive to O stars. Therefore, a population with strong PAH emission is not likely to have

ongoing star formation but instead will have formed stars recent enough to still contain B stars, which is less than approximately 100 Myr. This is consistent with earlier work (Davies et al. 2007) and with our conclusion that there is recent, but not ongoing, star formation with an age since the last active star formation of less than a few 100 Myr.

7. MOLECULAR OUTFLOWS

Three of the five active galaxies in our sample (NGC 7743, NGC 5643, and NGC 6300) show spatially resolved molecular gas flowing out from the AGN, and a fourth (NGC 3227) shows strong disturbances such as high dispersion associated with the ionized outflow although it is unclear whether the H_2 itself is outflowing. In two of these cases, the outflow exhibits the classical bi-cone morphology. For the fifth AGN, NGC 6814, it is not possible to say whether or not there is molecular outflow due to the limited field over which we can detect 1-0 S(1) line emission. However, we note that the 3D geometry of the ionized outflow (Müller-Sánchez et al. 2011) shows that it intersects the disk plane to the southwest, so that based on the discussion below and with higher signal-to-noise data, one might expect to see a molecular outflow also in this galaxy.

A property they all have in common is that the orientation of the outflow is such that it intersects, or has its edge close to, the galaxy disk. Our sketch in Figure 14 of the geometry for NGC 7743 shows that the (redshifted) far edge of the southern outflow and (blueshifted) near edge of the northern outflow are close to the galaxy disk. The geometrical model of Fischer et al. (2013) for NGC 5643 indicates that the (redshifted) far edge of the approaching outflow to the east is close to the disk, as is the (blueshifted) near edge of the western outflow. The outflow in NGC 6300 appears almost edge-on. Because it is aligned nearly along the minor axis of the host galaxy, it too must intersect the host galaxy disk. The ionized outflow in NGC 3227 also encloses part of the galaxy disk, in such a way that, if gas clouds in the disk were accelerated outward, these would be blueshifted to the west and redshifted to the east (Fischer et al. 2013). While the non-circular velocities of only $\sim \pm 20 \text{ km s}^{-1}$ in the central $1''\text{--}2''$ of NGC 3227 are modest, they are consistent with this geometry.

These results suggest that a minimum requirement for a molecular outflow must be that there is sufficient ambient molecular gas to be swept up by the wind from the AGN, and for a Seyfert nucleus residing in a disk galaxy, the most abundant source of ambient gas is the disk itself. It therefore seems likely that for a Seyfert galaxy to drive molecular gas outward, the outflow must be tilted over sufficiently far that it is close to, or intersects, the disk plane. This may occur rather commonly, given that outflows are oriented randomly with respect to the host galaxy (Clarke et al. 1998; Nagar & Wilson 1999; Kinney et al. 2000) and that they have a finite opening angle. Adding together the θ_{max} and β parameters derived by Fischer et al. (2013) yields the angle between the normal to the disk plane and the edge of the ionization cone in the objects they modeled. In 9 of 17 cases, the cone does indeed intersect the disk, and another 2–4 (allowing for a tolerance of $10^\circ\text{--}20^\circ$) come close. Thus we may expect more than half of Seyfert galaxies to drive molecular outflows. The key questions for these are how much mass is entrained, and how fast are they flowing?

To address these, we have identified regions in the three galaxies where outflowing H_2 is seen based on dispersion and residual velocity (except for NGC 6300 where it is based on the residual flux), and measured the 1-0 S(1) luminosity in these regions as

Table 6
Properties of Outflowing Gas

Galaxy	v_{out} (km s^{-1})	σ_{out} (km s^{-1})	$L_{\text{out}}^{1-0\text{S}(1)}$ ($10^4 L_\odot$)	$R/\langle \cos \theta \rangle$ (pc)	\dot{M}_{out} ($M_\odot \text{ yr}^{-1}$)
NGC 5643	60–80	90–100	3.0	250	10
NGC 6300	60–90	100–120	5.3	170	30
NGC 7743	~ 40	70–90	0.8	115	5

Notes. Column 1: object name; Column 2: the range or typical value, in the residual velocity field associated with the outflow; Column 3: the range, or typical value, in the dispersion map associated with the outflow; Column 4: luminosity in 1-0 S(1) line associated with the outflow (locus is based on v_{out} and σ_{out} except for NGC 6300 where it is based on the residual flux directly); Column 5: root-mean-square distance from nucleus to locus associated with outflow, adjusted to take account of the unknown outflow orientation; Column 6: outflow rate calculated as MV/R .

well as their rms distance from the nucleus. The typical values for these parameters are reported in Table 6. We have derived a characteristic outflow speed as $V \sim \sqrt{v_{\text{out}}^2 + \sigma_{\text{out}}^2} / \langle \sin \theta \rangle$ taking $\langle \sin \theta \rangle = \langle \cos \theta \rangle = 0.7$ to account for the unknown orientation of the outflowing H_2 (note that this correction is also applied to the distance of the outflowing gas from the AGN). This gives values in the range $130\text{--}190 \text{ km s}^{-1}$. To estimate the mass of molecular gas, we have derived the mass of hot gas from the luminosity of the 1-0 S(1) line in the relevant regions of the residual flux maps, assuming the molecules are thermalized at 2000 K and applying a scaling factor based on $M_{\text{cold}}/M_{\text{hot}}$. On large scales in star forming galaxies, this ratio is typically $10^{6.3}$ to within a factor of a few (Dale et al. 2005; Müller-Sánchez et al. 2006). We note that estimating a total gas mass from the residual 1-0 S(1) luminosity in NGC 3368 using this ratio yields a mass of $1\text{--}2 \times 10^7 M_\odot$ consistent with our other estimates in Section 5. On scales of a few hundred parsecs or less, this ratio may be smaller, in the range $10^{5.5}\text{--}10^{6.2}$ (Mazzalay et al. 2013); and there are indications that this may also be the case for Seyferts (Dale et al. 2005). As such, in order to avoid overestimating the total gas mass, we have adopted a ratio of $10^{5.5}$. This highly uncertain step yields masses in the range $5\text{--}25 \times 10^6 M_\odot$. A final step gives the outflow rate as $\dot{M}_{\text{out}} = MV/R$, yielding rates of order $10 M_\odot \text{ yr}^{-1}$.

Based on these order-of-magnitude calculations, we conclude:

1. The H_2 outflow speeds of around 150 km s^{-1} are lower than the outflow speeds of ionized gas, which are mostly in the range $200\text{--}2000 \text{ km s}^{-1}$ (Müller-Sánchez et al. 2011; Fischer et al. 2013; Storchi-Bergmann 2014). This difference may be because, as gas clouds are accelerated outward, an increasing fraction of the clouds are ablated and ionized, in which form the gas is more easily accelerated (large filling factor, lower density), which is why one sees higher velocities for the ionized gas. We have estimated the escape velocities of these three galaxies from the radial distances given in Table 6, deriving the galaxy mass from the H -band magnitude given in Paper I. We find $V_{\text{esc}} \sim 1500 \text{ km s}^{-1}$. This demonstrates that, unless it is continuously accelerated, the outflowing molecular gas cannot escape and will instead fall back,
2. The H_2 outflow rates, although rather uncertain, could be sufficiently high to have an impact on the local environment depending on how long the central black hole is active. For an activity timescale of $1\text{--}10 \text{ Myr}$, the AGN could drive $10^7\text{--}10^8 M_\odot$ of gas outward. However, as argued above,

this is likely to fall back again; it is certainly not enough to impact the large-scale properties of the host galaxy.

3. The median outflow speed of molecular gas (based on the 119 μm OH line) reported by Veilleux et al. (2013) of $\sim 200 \text{ km s}^{-1}$ for ULIRGS and QSOS is similar to that derived above for these few Seyferts. However, it is not clear whether one can compare the outflows from ULIRGS/QSOs to those from Seyferts due to the very different nature of the host system. It is notable that the molecular outflow rates derived by Sturm et al. (2011) for a small number of those ULIRGs/QSOs are 1–2 orders of magnitude greater than the rates we derive.

8. GAS INFLOW TO GALACTIC NUCLEI

In this section, we discuss the link between gas inflow mechanisms that might fuel AGNs, the properties of the host galaxy, and the environment.

8.1. Circumnuclear Structures in Our Sample

8.1.1. Two Modes of Gas Inflow to the Central Tens of parsecs

When analyzing individual galaxies in our sample in Section 5, we found gas kinematics consistent with inflow caused by bars and nuclear spirals in all three active galaxies in which inflow can be separated from outflow. Numerical models show that such inflow can be sustained for long timescales in a quasi-steady state (e.g., Maciejewski 2004). However, we also found that in both galaxies classified as inactive in which we detected warm molecular gas, a counter-rotating gas component is present. Counter-rotation requires reversion of the angular momentum vector from that of gas co-evolving with the galaxy disk, and this implies a dramatic change in velocity. For this reason, physical processes internal to the galaxy are unlikely to provide enough energy to bring about this change for large quantities of gas. On the other hand, accreted gas can naturally account for counter-rotation if its intrinsic angular momentum is significantly different from that of the disk. Therefore counter-rotation likely points at external accretion. External accretion likely occurs in the form of stochastic events, which happen on shorter timescales than the internally driven gas inflow that we observe in the active galaxies. If AGNs can be fed by external accretion, then there are two major consequences of this difference for the detectability of such process. First, there is a higher chance to see an AGN fed by internally driven gas inflow than by external accretion. Second, galaxies with external accretion onto the nucleus, which are likely to become active within a short timescale, may currently be classified as inactive.

We postulate that there are two distinct kinds of processes that drive gas inward to feed an AGN: (1) internal secular inflow that is quasi-continuous for long timescales and (2) stochastic external accretion events. It is likely that these have different duty cycles and manifest in different types of galaxies and environments. In particular, external accretion is unlikely to occur when there is no supply of cold gas external to the galaxy. This may apply either to isolated galaxies, or to galaxies in clusters or in large, evolved groups with X-ray cores. Also, a large reservoir of native gas in a galaxy may mask the signature of external accretion by reducing its impact and also influencing how easily it can be seen—this may be happening in at least one of our targets (NGC 3227). With a plentiful internal supply of gas, secular processes can dominate the inflow (Morganti et al. 2006; Young et al. 2011). Thus, the prevalent mechanism of accretion onto the nucleus is related primarily

to the environment and gas content of the galaxy, rather than to the galaxy classification. Despite this, the morphological classification is important, because it broadly reflects whether the host galaxy is likely to have internal gas, and it roughly correlates with the environment. We note, however, that the correlations are coarse and, for example, there is a significant population of blue early type galaxies with substantial gas reservoirs (Kannappan et al. 2009; Wei et al. 2010).

8.1.2. Possible Feeding of AGNs by Externally Accreted Gas

It is well known that a significant fraction of gas in early type galaxies is of external origin (Sarzi et al. 2006; Davis et al. 2011). The idea that the nuclear activity in early type galaxies is sustained by externally accreted gas has been proposed by Simões Lopes et al. (2007), who showed that for early type galaxies, all active galaxies have circumnuclear dust structures while only a small fraction (26%) of inactive galaxies do. This is in contrast to the late type galaxies in their sample, all of which, active and inactive, have dust structures. This result indicates that circumnuclear dust structures (tracing gas) are a necessary, but not sufficient, condition for fueling a central massive black hole. Simões Lopes et al. (2007) postulated that for early type galaxies the gas might be accreted from external sources, in contrast to late type galaxies where the large-scale disk provides an internal source of gas. Martini et al. (2013) pursued this hypothesis, looking at the spectral energy distributions and dust masses of 38 early type galaxies. They argued that although there is evidence for circumstellar dust around evolved stars, this could not account for the total dust mass in galaxies that exhibit dust structures. They proposed that for these objects, the dust is seeded by external accretion and continues to form in the accreted cold gas over long timescales, accounting for the observed gas masses.

Our observations show that if gas counter-rotating with respect to the stellar component (and to the native gas) implies its external origin, then such external counter-rotating gas can reach the innermost tens of parsecs of galaxies. This is seen in two galaxies (IC 5267 and NGC 3368) of our sample. Gas in the nucleus appears to form dynamically unstable configurations which are bound to result in an eventual rapid loss of angular momentum, with gas falling onto the galaxy center. Thus it is likely that gas inflow to the nucleus will follow the accretion event. Depending on the timescale over which this occurs, and also on whether these are isolated accretion events, these inactive galaxies may either become AGNs in the future (i.e., they are “pre-AGN”) or, due to rapid variability of inflow on the smallest scales, are currently in a short “off” cycle of an ongoing AGN phase. In assessing which of these scenarios is more likely, we recall that while the analysis of our targets in Paper I revealed systematic differences between the active and inactive galaxy samples, there was not such a clean separation for individual sources. Thus, even in the circumnuclear region where the dynamical timescale is 2–3 Myr, we may not have fully overcome the problem of timescale matching.

We note that rapid (i.e., 1–10 Myr) variability particularly affects inactive control samples, and a mismatch of the timescale between this and other factors that may influence AGN activity has a major impact on how such samples should be interpreted. This can most easily be realized with a simple thought experiment in which one hypothesizes that some aspect of the host galaxy or environment is responsible for triggering inflow. This may influence the galaxy for more than 1 Gyr; the resulting accretion onto the central black hole will occur at some point

Table 7
Summary of H₂ Phenomena, Dust Structures, and Environment

Galaxy	Rotating Disk	Circumnuclear Spiral	Perturbed	Outflow	Dust ^a	Environment ^b
NGC 3227	X	X		(X) ^c	C	Group of 13–14
NGC 5643	X	X		X	GD	Isolated
NGC 6300	X			X	C	Undisturbed, group of 9
NGC 6814	X				GD	Isolated
NGC 7743	X	X		X	LW	Undisturbed
IC 5267	X		X		C	Group of 11–14
NGC 4030					TW	Undisturbed; group of 4?
NGC 3368	X		X		CS	Group of 9–14
NGC 628					N	Undisturbed; group of 7?
NGC 357					N	Undisturbed; group of 6?

Notes. Summary of whether the following phenomena have been observed in the H₂ line distribution and kinematics within the central few hundred parsecs: the presence of a rotating disk, signs of inflow driven by a circumnuclear spiral, evidence for perturbing events, and detection of outflowing molecular gas. The lack of a mark indicates only that a particular structure is not traced by the 1-0 S(1) H₂ line in our data; it may still be apparent from maps of other tracers such as the Br γ line or dust structure.

^a Circumnuclear dust structure as classified by Martini et al. (2003): GD = grand design spiral, TW = tightly wound spiral, CS = chaotic spiral, C = chaotic, N = no dust structure.

^b Group membership as discussed in Section 3 (primarily from Garcia 1993 and Crook et al. 2007; see the text for full details of references). A question mark indicates where there is some uncertainty about membership (e.g., because of the different definitions used to classify groups).

^c The H₂ is disturbed (high dispersion) as a result of the outflow, but we do not directly see signs that the H₂ itself is outflowing (non-circular velocities are modest).

during this phase, but only on and off within a ~ 100 Myr period. If one then takes a snapshot to look at which galaxies are active and inactive, one will see only a random subset, which will be different for another snapshot. Based on any of these snapshots, although the host galaxy or environmental factor will accompany AGN fueling, the conclusion from the control sample would be that one does not lead to the other, which contradicts the initial hypothesis of the thought experiment.

8.1.3. Minor Mergers versus Intergalactic Gas

In the literature, external accretion is usually associated with dwarf satellites falling onto the host galaxy and releasing their gas to the host. However, in the particular case of NGC 3368, there is an intergalactic H I bridge leading to NGC 3368 (Michel-Dansac et al. 2010). Because of the lack of non-uniformities in the circumnuclear stellar kinematics, we postulate that accretion of gas rather than stellar systems—i.e., streamers rather than (minor) mergers—is likely to play a role in this particular case, and that streamers may provide an additional source of external gas, besides the commonly considered mergers.

There is some evidence from H I observations to support this. Kilborn et al. (2009) found that the H I mass function in groups is flatter than in the field, and that there is a lack of high H I mass galaxies in groups. They suggested this may be due to tidal stripping of gas from disk galaxies through interactions, rather than the result of ram pressure stripping, which occurs in clusters but is not so important in groups. Wilcots (2009) argued that galaxies falling into groups are experiencing the impact of a dense environment for the first time, and that the transformation of galaxies and the intergalactic medium (IGM), often referred to as pre-processing, may take place in the group environment prior to infall of the group into a cluster. There is, however, a maximum group size in which such pre-processing occurs. Hess & Wilcots (2013) found that as group membership increases from 5 to 20, two things happen: the fraction of H I galaxies decreases and those with H I tend

to be less centrally concentrated. Their results suggest that groups with 5–20 members are an ideal place for H I to be stripped away from the outskirts of galaxies into the IGM, and hence be available (still as neutral gas) to accrete onto other galaxies in the group. While this could provide a source of atomic gas in the local environment, further work is needed to investigate whether the origin of counter-rotating molecular gas in IC 5267 and NGC 3368 is related to stripping of H I from the outskirts of galaxies. We note that intragroup molecular gas has been observed, but only in strongly interacting groups such as Stephan’s Quintet (Lisenfeld 2002).

8.1.4. Trends in Our Sample

When assessing the conditions that are favorable to internally versus externally driven circumnuclear inflow, we use a combined sample containing all our galaxies, rather than separating them according to whether they are specifically active or inactive at the current time. We relate the H₂ morphology and kinematics reported in Section 5 to the environment discussed in Section 3 and the circumnuclear dust structures reported by Martini et al. (2003). These properties are all summarized in Table 7, and enable us to make the following points:

1. There are three galaxies without 1-0 S(1) detections: NGC 4030, NGC 628, and NGC 357. They are either isolated or in small groups with <10 members, and two show no circumnuclear dust structure. All three undisturbed galaxies without circumnuclear molecular disks are inactive.
2. All four galaxies with chaotic dust structure (designated C or CS) reside in groups with ~ 10 –15 members. They are two inactive galaxies IC 5267 and NGC 3368, and two AGNs NGC 3227 and NGC 6300. The chaotic dust structure may either reflect the H₂ distribution and kinematics which are perturbed by external accretion (leading to counter-rotating gas structures), or be superimposed on an internal mechanism revealed by the H₂ such as bar driven inflow.

3. The remaining three AGNs are isolated or have undisturbed large-scale disks: NGC 5643, NGC 6814, and NGC 7743. All three of these undisturbed AGNs have circumnuclear dust structures classed as spirals (GD, LW, TW) as well as circumnuclear molecular disks.

These point to a scenario in which (1) a circumnuclear spiral in an undisturbed galaxy with plentiful gas supply is a sign of secular internal inflow of gas to the nucleus, and (2) chaotic circumnuclear dust structures indicate external accretion: they are preferentially happening in galaxies that are part of a moderate-size group with 10–15 members, and in Section 8.1.3 we showed that in groups of similar size, H I stripped from the outskirts of galaxies could provide a source of intergalactic gas.

8.2. Comparison to Other Samples

The small number of targets limits the statistical robustness of our results because it cannot properly sample the full range of galaxy hosts (Hubble type and presence/absence of a bar). As such, we now extend our analysis to look at other samples of matched pairs of active and inactive galaxies that were observed using integral field spectroscopy (IFS) so that the stellar and gas kinematics are spatially resolved. We examine first the samples of Dumas et al. (2007), in which nearly all galaxies are late type, and of Westoby et al. (2012), in which the majority of the galaxies are early type. For these two samples, which between them provide more than 30 additional sources, the spatial scales probed extend out to beyond 1 kpc at resolutions of 100–600 pc. In this part of the analysis, we focus on the kinematic evidence for a relation between the inflow mechanism and host galaxy type. Because there is no sharp dividing line that separates host galaxy types into two distinct groups, we use the terms “early type” and “late type” loosely. Specifically, for the purpose of this analysis, we take galaxies classed as Sa or earlier to be “early” and Sab or later to be “late.”

We do not attempt a detailed study of the kinematics but look at whether the gas and stars are co-rotating or counter-rotating, how this is related to the host type, and if it indicates whether external accretion or secular evolution is at work. We then turn to the sample of Mazzalay et al. (2014) in which all galaxies are late types, but several of them are in a cluster environment. We take a brief look at whether this has an impact on their circumnuclear structures.

8.2.1. Secular Internal Inflow

When secular evolution is driving gas inflow, the gas and stars are expected to be co-rotating. On the other hand, in the external accretion scenario, the accreted material should show no preference for co- or counter-rotation with respect to the pre-existing stellar population. In their analysis, which included seven pairs of matched active/inactive galaxies, Dumas et al. (2007) reported the difference in mean P.A. between the ionized gas and stars. Interestingly, the galaxy with the largest discrepancy between these is the AGN NGC 2655. This S0/a galaxy is known to have off-planar gas and complex dust structures (Erwin & Sparke 2003), and is in a group with four to seven members (Garcia 1993; Crook et al. 2007). In contrast, the galaxies in the other six matched pairs are all morphological type Sab to Sbc. None of the six inactive late types showed evidence for misalignments between the stellar and gas kinematics: in all of them, the gas and stars are co-rotating. Although three of the six active late types did have

misalignments, their range of 25–55° indicates the gas and stars are still co-rotating. Thus, interactions and external accretion might play a role here, but it is also possible that internal processes such as bar-driven inflow (NGC 4151 and NGC 4579 are both barred and have circumnuclear rings) could generate these moderate misalignments. We note that in the case of NGC 5194, the [O III] line from which the gas kinematics were derived appears to be influenced by the outflow (Cecil 1988; Terashima & Wilson 2001); the H β kinematics are more closely aligned with the stellar kinematics.

We recall that in our sample, there were three AGNs with undisturbed hosts, circumnuclear molecular disks, and circumnuclear spiral dust structures. Of these, NGC 6814 and NGC 5643 are classified as Sbc and Sc; NGC 7743 is an S0. NGC 3227, an interacting Sa galaxy with a chaotic dust structure, also exhibits unambiguous spiral driven inflow. We have shown that the presence of a bar can play a key role in generating these structures. We argue below that the presence of a bar and a plentiful supply of gas in a large-scale disk may be more important than the host type in understanding such galaxies. Archetypal examples of this sort of AGN host may be Narrow Line Seyfert 1s (i.e., type 1 AGNs with a “narrow” broad line region with FWHM < 2000 km s⁻¹). In terms of bulge properties, these AGNs appear to lie at the extreme end of the range covered by type 1 AGNs in general, having pure pseudo-bulges (Orban de Xivry et al. 2011; Mathur et al. 2012). The implication is that they have evolved in relatively isolated environments without major mergers. Orban de Xivry et al. (2011) also brought together studies in the literature which show that these are associated with strong bars, enhanced circumnuclear star formation, and grand design circumnuclear spirals: all are indications of secular evolution bringing gas inward from the large-scale disk. In these objects, the bar drives gas into the circumnuclear region as well as stimulates the formation of the circumnuclear spiral, and it is the circumnuclear spiral that brings gas to smaller scales, enabling it to fuel the AGN. For these AGNs, gas inflow is internally driven, and does not appear to result from external accretion.

One important question is what inflow rates can internal secular evolution drive? An example we can turn to is NGC 1097, which has a strong bar, a pseudo-bulge, and circumnuclear spiral structure. H I observations indicate the only interaction is with its dwarf companions NGC 1097A which has $M_{\text{H I}} < 10^6 M_{\odot}$, or NGC 1097B which has $M_{\text{H I}} = 5 \times 10^6 M_{\odot}$ (Ondrechen et al. 1989; Higdon & Wallin 2003). The inflow rate to the central 10–20 pc has been estimated to be of order $0.05 M_{\odot} \text{ yr}^{-1}$ (Davies et al. 2009). Given that much of this gas turns into stars at that radius, and inflow to smaller scales is still likely to be inefficient, this is unable to power a luminous Seyfert. Indeed, the AGN’s 2–10 keV luminosity of $6 \times 10^{40} \text{ erg s}^{-1}$ (Lutz et al. 2004) is moderate. Thus, while secular processes can provide the gas inflow required, the inflow rate, and hence accretion rate onto the black hole, is modest. In contrast, much higher inflow rates of 0.1–1 M_{\odot} have been reported by Storchi-Bergmann (2014) for a variety of LINER and Seyfert galaxies. It is not yet clear whether these can be achieved through spiral driven inflow alone, or if some perturbation (internal or external) is required to temporarily enhance the inflow rate, as appears to have happened in the luminous Seyfert NGC 1068. In this galaxy, Müller-Sánchez et al. (2009) showed that in the central ~ 100 pc, clouds inflowing along the circumnuclear bar collide with clouds swept up at the edge of an expanding cavity, leading to gas falling almost directly toward the AGN at a high rate.

8.2.2. Stochastic External Accretion

Stochastic external accretion is most easily detected in early type galaxies, as on average they contain less gas than the late types. It may provide a natural explanation for why in the Westoby et al. (2012) sample, emission from ionized gas was detected in all 10 early type active galaxies but was not (or only weakly) detected in four of the five early type inactive galaxies: the inactive galaxies are inactive simply because they have not recently accreted gas and do not have their own internal supply. This sample includes 21 galaxies (14 active and 7 inactive) with morphological classifications, of which 15 (10 active and 5 inactive) are classified as S0 to Sa.¹⁰ Stellar kinematics could be measured in 11 of these 15 early type galaxies, and 7 of these show clear signs of stellar rotation. Of these, which are all AGNs, five have co-rotating $H\alpha$ and two have counter-rotating $H\alpha$. In contrast, all four of the late type (Sab or later) galaxies in which stellar kinematics could be measured show clear stellar rotation with co-rotating $H\alpha$ (we note that, possibly due to their shorter integration times, in neither of the inactive late-type galaxies could stellar kinematics be measured, and neither had good $H\alpha$ detections). While the numbers involved are still small, these results suggest that the Westoby et al. (2012) sample upholds the following observational signatures of external accretion (of intergalactic gas, or minor mergers) as a source of the gas fueling AGNs: (1) the paucity of gas in most inactive early type galaxies contrasting with the presence of gas in all active early types and (2) the existence of at least some early type galaxies with counter-rotating gas. The fraction above ($\sim 30\%$) of early type galaxies in which the gas is counter-rotating with respect to the stars is similar to that reported by Sarzi et al. (2006) for the SAURON sample of galaxies, and also by Davis et al. (2011) for the larger and complete ATLAS^{3D} sample. We note that both of these samples cover the central few kiloparsecs at a sampling of 100–200 pc.

8.2.3. Cluster versus Group Environment

Davis et al. (2011) show that for the ATLAS^{3D} sample of early type galaxies, there are few misalignments for galaxies in the Virgo Cluster while there are numerous misalignments in “field galaxies” (i.e., including isolated galaxies as well as those in groups). We have argued above that misalignments due to external accretion occur in *group* environments, rather than *cluster* environments. The reason was already given by Davis et al. (2011): intra-cluster gas is heated and so the source of external atomic or molecular gas is curtailed. These authors find that the kinematic misalignments occur exclusively in galaxies residing in environments whose density is below a critical local density limit, corresponding to a number density of $\sim 20 \text{ Mpc}^{-2}$, which includes moderately dense groups.

Mazzalay et al. (2014) present an analysis of the circumnuclear H_2 properties of six late type (Sab or later), mostly barred, galaxies. While half of them lie in groups, the other half is in the core of the Virgo cluster and hence provides an opportunity to assess circumnuclear properties in the cluster environment. Below, we briefly look at all six of their galaxies in the context of environment.

NGC 3351 and NGC 3627 are both in the Leo I group (which has 9–14 members, Garcia 1993; Crook et al. 2007) and have large neighbors 60–130 kpc away. Despite this, the former appears undisturbed on large scales, while the latter

is interacting. NGC 4536, while formally belonging to the Virgo cluster, is in a sub-group located about 3 Mpc from the cluster center. Like the first two galaxies, it has a similar sized companion 120 kpc away, and a small blue irregular galaxy 40 kpc away. The circumnuclear molecular kinematics for all three of these galaxies show circular or elliptical motions in their disk planes, which are consistent with being internally driven. NGC 3351, which is undisturbed and has circular motions, is an inactive galaxy with a limit on its 0.3–8 keV hard X-ray luminosity of $< 10^{38} \text{ erg s}^{-1}$ (Grier et al. 2011), suggesting that no inflow is occurring. For the other two, with elliptical motions, inflow may be happening at a low level: they are both AGNs, although only NGC 3627 has a measured 2–10 keV luminosity, which is $3 \times 10^{39} \text{ erg s}^{-1}$ (Brightman & Nandra 2011).¹¹

The remaining three galaxies—NGC 4569, NGC 4501, and NGC 4579—are all within 600 kpc of the Virgo cluster center, with different numbers of close companions, and varying signs of ram pressure stripping. All three are classified as AGNs. Both NGC 4579 and NGC 4501 have 2–10 keV luminosities of $10^{41} \text{ erg s}^{-1}$ within the range of our AGN sample, while NGC 4569 has a more modest hard X-ray luminosity of $3 \times 10^{39} \text{ erg s}^{-1}$ (Brightman & Nandra 2011).¹¹ The circumnuclear kinematics were all found to show streaming motions by Mazzalay et al. (2014), although for both NGC 4569 and NGC 4579 they were disordered, with complex kinematics and no indications of underlying ordered rotation. Only NGC 4501 showed circular rotation with streaming superimposed. Based on the linear features in the dust structure map (Simões Lopes et al. 2007), this is possibly of external origin.

Our conclusion from the Mazzalay et al. (2014) sample is two-fold: (1) even in a group environment, gas inflow in late type galaxies may still be driven by internal mechanisms, which can be understood if the mass of any accreted gas is much less than the gas mass already in the galaxy disk; and (2) the circumnuclear molecular gas kinematics of galaxies in clusters may be very complex, presumably because the extreme environment can have an impact even deep in the potential well of a galaxy.

Putting this together with the observations of H I in galaxy groups (Section 8.1.3) and the trends seen in our sample (Section 8.1.4), these results suggest that, in the context of fueling AGNs, external accretion appears to be a process that requires specific circumstances: a dense enough environment (i.e., a group with 10–15 members) to make streamers and/or minor mergers sufficiently likely, but not so dense (> 20 members) that gas in the IGM is predominantly shock-heated.

9. CONCLUSIONS

We present an analysis of the spatially resolved stellar and molecular gas kinematics and distributions for a sample of five pairs of matched active and inactive galaxies, covering their central few hundred parsecs. This has enabled us to study molecular inflows and outflows, with the aim of relating these to the large-scale host galaxy properties and the environment. We see a link among the local environment, the circumnuclear dust structures (which may also be caused by dust superimposed along the line of sight), and the circumnuclear H_2 structures/kinematics. The number of galaxies in our sample is too small for robust statistical conclusions, and so some of the main findings below require further confirmation:

¹⁰ Applying a cutoff at type S0, as was done by Martini et al. (2013), has no impact on the result of the analysis except to reduce the numbers of objects.

¹¹ The intrinsic 2–10 keV luminosities given in Brightman & Nandra (2011) have been corrected to the distances adopted by Mazzalay et al. (2014).

1. Circumnuclear molecular disks are seen in all five active galaxies but only two inactive galaxies, suggesting they are required for fueling Seyfert luminosity AGNs.
2. There are two modes of inflows feeding AGNs: secular processes and external accretion. The former is quasi-continuous for long timescales and takes place in galaxies with a plentiful internal supply of gas. The latter occurs in stochastic events and may bring in significant gas masses in a short time. It is revealed by counter-rotation in gas in the central few hundred parsecs that leads to dynamically unstable configurations.
3. In addition to minor mergers, externally accreted gas may be coming from streamers that form intergalactic filaments and bridges in groups observed in H I. In such cases, moderately dense groups (with 5–20 members) provide an environment conducive to external accretion, because of efficient stripping of gas from galaxies into the IGM there.
4. Circumnuclear spiral structures are associated with relatively isolated galaxies and indicate that the large-scale disk is the source of gas. On the other hand, chaotic circumnuclear dust structures appear to be associated with external accretion in groups. This difference is driven primarily by environment; the relation to galaxy type is a reflection of the intrinsic gas content of galaxies. Early type galaxies tend not to have a plentiful supply of internal gas and so the impact of external accretion is more easily seen.
5. For an AGN fueled by external accretion one can expect (1) paucity of gas in inactive galaxies versus presence of gas in active galaxies, (2) the existence of counter-rotating gas in the circumnuclear region of early type (i.e., intrinsically gas poor) galaxies, and (3) moderately dense local intergalactic environments. These characteristics appear to be supported by the matched active/inactive galaxy samples presented here, as well as in Dumas et al. 2007 and Westoby et al. 2012, and by early type samples (Sarzi et al. 2006; Davis et al. 2011).
6. Inactive control samples need to be assessed in the context of the relevant timescales. This is a particular concern if there is a mismatch between the timescale of AGN accretion events (which occur on sub-parsec spatial scales) and the timescale of large-scale phenomena (on kpc to Mpc spatial scales). The role of environment also needs to be considered (perhaps via proxies such as host type) when selecting and analyzing matched active and inactive samples.
7. There cannot be ongoing star formation in the central ~ 100 pc of either the active or inactive galaxies in our sample. We note this is consistent with the detection of PAH features in the centers of AGNs, if PAH emission is a signature of stars older than the ionizing stars traced by H-recombination lines.
8. Spatially resolved molecular outflows are found in three or four of the five active galaxies, but none of the inactive galaxies. In these galaxies, the outflow (ionization) cone is tilted over far enough that it intersects the host galaxy disk, which we argue is the source of ambient molecular gas being expelled.
9. The molecular outflow speeds of ~ 150 km s $^{-1}$ are less than the 200–2000 km s $^{-1}$ typical of ionized gas, and well below the escape velocity of the galactic potential so that the gas is likely to fall back. The outflow rates are of order $10 M_{\odot}$ yr $^{-1}$. While this is high enough to have an impact on the circumnuclear interstellar medium, it is not enough to impact the large-scale properties of the host galaxy.

The authors are grateful to those who generously agreed that we could make use of their data: Paul Martini for sharing his *HST* data for each of the galaxies in our sample; Sebastian Haan for sharing his CO 2-1 and CO 1-0 data for NGC 3368; and Leslie Hunt and Matt Malkan for sharing their data and analysis of Seyfert, LINER, starburst, and normal galaxies. We thank the referee for a thorough reading of the paper and for making a variety of suggestions that have helped to improve it. This research has made use of the NASA/IPAC Extragalactic Database (NED) which is operated by the Jet Propulsion Laboratory, California Institute of Technology, under contract with the National Aeronautics and Space Administration. E.K.S.H. acknowledges support from the National Science Foundation Astronomy and Astrophysics Postdoctoral Fellowship under award AST-1002995, as well as support from the NSF Astronomy and Astrophysics Research Grant under award AST-1008042.

Facility: VLT:Yepun

APPENDIX

ORIENTATION AND LARGE-SCALE STRUCTURAL PROPERTIES OF INDIVIDUAL GALAXIES

In this Appendix, we derive the kinematic major axis P.A. and inclination (i) for each galaxy. The aim is to find the appropriate values to adopt for our analysis. On small scales, we use two methods. The first makes use of kinemetry (Krajnović et al. 2006) to quantify the stellar kinematics. We apply this method globally to the CO 2-0 velocity and dispersion simultaneously to all radii over which at least 75% of an ellipse can be measured, and adjust the P.A. in order to minimize the absolute value of the A_1 parameter (see Krajnović et al. 2006). We note that, as expected, this yields very similar values to those derived using the method described in Appendix C of Krajnović et al. (2006) since it is based on the same concepts and differs only in the detail of its implementation. The second method is based on the stellar distribution, fitting elliptical isophotes to a map of the CO 2-0 bandhead flux. For this, we made use of the multi-Gaussian expansion method (Emsellem et al. 1994), using the fitting method described in Cappellari (2002) to parameterize galaxy surface brightness profiles. As for the kinematics, the aim was to find single global estimates for the P.A. and i based on the data within our FOV. However, there can be large uncertainties in the derived P.A. and i , and also large differences between the kinematic and isophotal P.A. or i . In order to provide crucial guidance in such cases, we first assess the large-scale properties of each galaxy. The notes below compare the large and small scales, providing a rationale for the values adopted in our analysis, which are given in the second column of Tables 3 and 4.

A.1. NGC 3227

Determining the global orientation of NGC 3227 with precision is difficult, partly because the presence of a large, strong bar means that gas (and possibly stellar) kinematics may be somewhat non-circular in much of the visible disk, and also because it is interacting strongly with its elliptical-galaxy neighbor NGC 3226 and with a nearby gas-rich dwarf galaxy (which may in fact be a tidal dwarf resulting from the interaction; Mundell et al. 1995, 2004). Nevertheless, a combination of published two-dimensional (2D) gas and stellar kinematics implies a consistent P.A. for the LON and weaker constraints on the galaxy inclination. Mundell et al. (1995) found from their analysis of

VLA H I data that the main gas disk was “really quite undisturbed,” with a kinematic P.A. of $158 \pm 2^\circ$; they estimated an inclination of 56° from the shape of the H I isophotes (excluding the extended plumes to the north and south which are probably tidal features due to the interaction). The tilted-ring analysis of ^{12}CO data by Schinnerer et al. (2000) indicated a kinematic P.A. of $160^\circ \pm 2^\circ$ and an inclination of 56° , almost identical to the H I analysis. Finally, Dumas et al. (2007) found a stellar-kinematic P.A. of $160^\circ \pm 5^\circ$ from their analysis of a SAURON stellar-velocity field; this is consistent with the stellar-kinematic PA of 157° reported by Barbosa et al. (2006) based on higher-resolution, smaller-scale Gemini/GMOS IFS data. Taken all together, this suggests a LON with PA $\approx 159^\circ$, and a somewhat less certain inclination of $\sim 56^\circ$. The P.A. of the bar is very similar to that of the disk; we estimate it at $\sim 155^\circ \pm 5^\circ$, based on the *K*-band image of Mulchaey et al. (1997) and an archival Spitzer IRAC1 image (Gallimore et al. 2010).

On small scales, our data show a strong stellar velocity gradient, so that the kinematic P.A. is well determined at 155° . Because it is comparable to the P.A. on large scales, we adopt it. It is also consistent with that reported by Davies et al. (2006) for the circumnuclear ring at a radius of $1''.7$ (see Figure 4), which is completely within our field of view and is visible in our *K*-band data, as shown in the top panels of Figure 1. Assuming the ring is intrinsically round, its axis ratio suggests an inclination of 47° rather than the 56° characteristic of the large scales, and so we adopt that value. Although this assumption may not be strictly correct (the average deprojected ellipticity of such rings is in the range 0.1–0.2, Comerón et al. 2010), an error in inclination has only a small impact on our modeled velocity fields, for the same reason that deriving an inclination from a velocity field is associated with a large uncertainty. We note that the ring was also reported by Barbosa et al. (2006), who found its location corresponds to low stellar dispersion as measured in the Ca II triplet—an effect that can also be seen in the stellar dispersion measured from the CO 2–0 bandhead (Figure 4 of Paper I). We have overdrawn an ellipse with a semi-major axis of $1''.7$ and our adopted P.A. and i of 155° and 47° . The slightly different P.A. derived from the stellar isophotes could be due to a secondary bar which Baker (2000) and Schinnerer et al. (2000) proposed may exist on scales of 10–15".

A.2. NGC 5643

Various estimates based on the shape of the outer isophotes of this barred spiral galaxy suggest a global inclination of $\sim 23^\circ$ – 25° (Morris et al. 1985; García-Gómez et al. 2004; Li et al. 2011). Measurements of the P.A. of the outer isophotes yield estimates of $\sim 121^\circ$ – 128° (Morris et al. 1985; Li et al. 2011), roughly consistent with the kinematic major axis of 137° determined by Morris et al. (1985) from their Fabry–Perot H α velocity field. Thus on large scales we adopt a compromise P.A. of 129° (or equivalently -51°), while noting this is somewhat uncertain, and an inclination of 24° . Ellipse fits to the *K*-band image of Mulchaey et al. (1997) yield a bar P.A. consistent with their measurement of $\approx 85^\circ$.

In the circumnuclear region, we measure a difference in the stellar kinematic and isophotal P.A. and i , which may partially be explained by the bar. However, the rather circular isophotes also indicate that the stellar distribution is thick rather than disky on small scales, as would be expected from the $\sim 70 \text{ km s}^{-1}$ stellar velocity dispersion (Paper I). We therefore adopt the stellar kinematic values for P.A. and i , which are well constrained due to the large velocity gradient, bearing in mind that the small-

scale kinematics may be influenced by the bar. We note that the apparent excess of stellar continuum seen in Figure 1, especially to the east of the nucleus, may be due to reduced extinction in that region resulting from an outflow, similar to the situation reported for NGC 4945 by Moorwood et al. (1996) and Marconi et al. (2000). This is discussed more in Section 5.

A.3. NGC 6300

This barred spiral galaxy has been extensively studied by Buta and collaborators (Buta 1987; Ryder et al. 1996; Buta et al. 2001). The data presented in those papers, including multiple long-slit H α rotation curves, H I mapping, and Fabry–Perot H α maps, all suggest a consistent kinematic orientation with P.A. $\sim 109^\circ$ and inclination $\sim 50^\circ$; these values are also consistent with those derived from the shape of the outer isophotes. Analysis of an archival Spitzer IRAC1 image (proposal ID 80072) suggests a P.A. of $\approx 63^\circ$ for the bar.

The stellar kinematic and isophotal P.A. and i in the central few hundred parsecs are consistent with each other and also with those on large scales. As such, we simply adopt the values derived from our kinematic analysis of this region.

A.4. NGC 6814

This galaxy is very close to face-on; the presence of strong spiral structure makes determining the orientation from the outer isophotes difficult, since the measured P.A.s and ellipticities will be dominated by variations in local spiral arm strength. Based on a VLA H I velocity field, Liszt & Dickey (1995) found a kinematic P.A. for the optical disk ($r \lesssim 90''$) of 10° – 20° ; at larger radii, the H I disk appears to be warped. Unfortunately, they did not attempt to determine an inclination from the velocity field, but noted that it was probably less than 20° . Due to the uncertainty in P.A. and i from the isophotes and also due to the warp in the H I disk, we take the large-scale inclination to be $i = 21^\circ$ as reported in de Vaucouleurs et al. (1991), along with 15° as an estimate for the P.A.

On small scales, the modest stellar velocity gradient and fairly circular isophotes suggest that the inner region of this galaxies is also relatively close to face-on. Given the uncertainty of the P.A. on both large and small scales, the values are not vastly dissimilar, and so we simply adopt that derived from the small-scale kinematics. The small-scale stellar kinematic and isophotal estimates of i also differ, although this is again due to the significant uncertainties arising from the face-on nature of the galaxy. As such, we adopt i from large scales, which is similar to our isophotal value.

A.5. NGC 7743

This galaxy has a prominent bar with a visible box/peanut structure (Erwin & Debattista 2013) and a luminous lens surrounding the bar with a P.A. of $\sim 80^\circ$ – 90° , consistent with the RC3 P.A. However, Sloan Digital Sky Survey g , r , and i images, as well as the deeper *R*-band image of Erwin & Sparke (2003), show faint outer isophotes with a different orientation. This outer disk has a P.A. of $\sim 110^\circ$ and an ellipticity of ~ 0.22 , suggesting an inclination of $i \sim 39^\circ$ – 40° . This agrees quite well with the stellar kinematic analysis of Katkov et al. (2011), who analyzed a SAURON IFS stellar velocity field and three long-slit stellar velocity profiles and derived a kinematic P.A. of $\sim 120^\circ$ and an inclination of $i = 40^\circ \pm 2^\circ$. Our compromise estimate is a P.A. of $\sim 115^\circ$ (or equivalently $\sim -65^\circ$) and an inclination of 40° .

In the central few arcsec, we measure a P.A. and i from both stellar kinematics and isophotes that are remarkably consistent with those on large scales, supporting the conclusion in Section 3 that it is an undisturbed galaxy. The stellar velocity gradient is significant enough that the kinematic P.A. is well-defined, and so we adopt this value. The inclination has some uncertainty, although this is not enough to have a significant impact on the modeled velocity field, and so again we simply adopt the value derived from the kinematics.

A.6. IC 5267

The P.A. of this galaxy is well-defined: we obtained a mean P.A. of $\sim 139^\circ$ from our ellipse fits to the isophotes from a Spitzer IRAC1 image (Sheth et al. 2010), consistent with the mean value of 137° found by Li et al. (2011) from their I -band image. The inclination is somewhat less well-defined; the ellipticity of the IRAC1 isophotes varies from a low of ~ 0.15 to a maximum of ~ 0.30 (corresponding to inclinations of $\sim 33^\circ$ – 47°). The highest value is found in a region of partial spiral structure, and so may be affected by local star formation. We note that both Laurikainen et al. (2010) and Li et al. (2011) suggest inclinations of 34° – 38° , the former from a 2D bulge/disk decomposition of a K -band image and the latter as a mean from I -band ellipse fits. There is no evidence for a bar in this galaxy; the spiral structure is tightly wrapped and flocculent, with two narrow, elliptical star-forming rings or pseudo-rings (semi-major axes $a = 78$ and $147''$) identified from $H\alpha$ imaging (Grouchy et al. 2010) and also apparent in UV images (Gil de Paz et al. 2007). The axis ratio of these rings also suggests an inclination around $\sim 40^\circ$.

The circumnuclear stellar velocity field shows almost no velocity gradient (Paper I), resulting in a highly uncertain kinematic P.A. Similarly, the circumnuclear stellar isophotes are rather circular, indicating that the inner region of the galaxy is face-on and/or that the stars in the central few hundred parsecs are predominantly in a spheroidal (or at least geometrically thick) distribution with little ordered rotational component. The high stellar dispersion of $\sim 160 \text{ km s}^{-1}$ reported in Paper I supports the latter option. For our purposes, the difference between the inclination measured on large and small scales is not critical because the H_2 velocity field clearly shows two distinct components, and we can model these directly without needing to subtract an underlying disk. As such, we adopt the P.A. from the circumnuclear stellar isophotes, and i from the large scales.

A.7. NGC 4030

This unbarred Sbc spiral has a moderately well-defined orientation, with literature estimates of the P.A. and inclination ranging from 20° – 38° and from 37° – 44° , respectively, in the compilation of García-Gómez et al. (2004); they adopt mean values of P.A. = 32° and $i = 40^\circ$ from their Fourier analysis approach. The SAURON stellar and gas kinematics presented in Ganda et al. (2006) are very regular and consistent with this overall orientation (e.g., inspection of their Figure 5 suggests a P.A. of $\sim 35^\circ$ for the stellar kinematic LON).

In the central few arcsec, the stellar kinematics and isophotes yield similar P.A. and i , which are also not very different from those on large scales.

A.8. NGC 3368

Nowak et al. (2010) undertook a detailed analysis of the orientation of this nearby, double-barred (Erwin 2004) spiral. From

the outer-disk isophotes they derived a P.A. of $\sim 172^\circ$, consistent with kinematic estimates from H I data (Schneider 1989; Sakamoto et al. 1999) and Fabry–Perot $H\alpha$ data (Sil’chenko et al. 2003). The shape of the isophotes suggested an inclination of $\sim 53^\circ$, roughly consistent with the Fourier analysis of Barberà et al. (2004) and with an inversion of the K -band Tully–Fisher relation using the observed Cepheid distance to the galaxy (see Nowak et al. 2010 for details). The P.A.s of primary and secondary bars are 115° and 129° , respectively (Erwin 2004).

In the central few hundred parsecs, we find a large discrepancy between the stellar isophotal P.A. and the stellar kinematic P.A. This is due to its small scale bar (Knapen et al. 2003; Erwin 2004; Nowak et al. 2010) for which such an offset is typical. However, the kinematic P.A. is effectively the same as that at large scales, so we adopt it. Because of this, and due to the uncertainty in i as derived from kinematics, we also adopt i from large scales. We note also that Figure 1 appears to indicate a slight excess of stellar continuum to the west of the nucleus. That there is no equivalent feature in the stellar kinematics could be because it contributes only 20%–25% of the total stellar continuum at that location. It could result from either a stellar population associated with the gas condensation that we discuss in Section 5, or a distortion of the central stellar population by that condensation. In either case we can estimate an associated stellar mass from the luminosity of the excess, $L_K = 2 \times 10^6 L_\odot$, using mass-to-light ratios for different stellar populations. For continuous star formation over an age of 0.1–1 Gyr we find that the ratio of mass currently in stars (i.e., excluding both non-luminous remnants and gas that has been returned to the ISM) is 1 – $2.5 \times 10^6 M_\odot$. For an older 1–10 Gyr population that is no longer forming stars, the mass still in stars would be $\sim 5 \times 10^6 M_\odot$.

A.9. NGC 628

The VLA H I mapping of Kamphuis & Briggs (1992) showed regular rotation in a nearly face-on main disk ($r \lesssim 380''$), with a P.A. of 25° and an assumed inclination of 6.5° , along with evidence for warping of the H I disk at larger radii. The more recent analysis of *The H I Nearby Galaxy Survey* (THINGS) H I data by Tamburro et al. (2008) yielded $i = 7^\circ$ and a P.A. of 20° for the main disk, consistent with the P.A. of $19^\circ \pm 7^\circ$ found from analysis of Fabry–Perot $H\alpha$ data by Fathi et al. (2007). Since isophotal analysis of galaxies this close to face-on can be easily confused by the distorting effects of spiral arms, the best estimate is that from the gas kinematic observations, $i = 7^\circ$ and P.A. = 20° .

The lack of stellar rotation in the central few arcsec of this galaxy is consistent with its nearly face-on appearance at large scales. The low stellar dispersion ($\sim 30 \text{ km s}^{-1}$, Paper I) suggests that this is due to its orientation rather than because the stars are in a spheroidal distribution. As such, the P.A. and i remain uncertain. But because there is no measurable stellar velocity gradient, and also no 1-0 S(1) line emission, we do not model this galaxy at all and so do not adopt any specific P.A. or i for the circumnuclear region.

A.10. NGC 357

Although there are no published 2D kinematics for this double-barred galaxy, the outer disk is symmetric and apparently undisturbed. The deep I -band image of Aguerri et al. (2005) yields a consistent P.A. of 20° (or equivalently $\sim -160^\circ$) and an inclination of 37° . The P.A.s for the primary and secondary bars are 120° and 45° respectively (Erwin 2004).

In the central few hundred parsecs, the stellar kinematic P.A. matches that at large scales closely. However, the isophotal P.A. differs, suggesting a triaxial system. As such, we have adopted i from large scales.

REFERENCES

- Aguirri, J., Elias-Rosa, N., Corsini, E., & Muñoz-Tuñón, C. 2005, *A&A*, 434, 109
- Arnold, T., Martini, P., Mulchaey, J., Berti, A., & Jeltema, T. 2009, *ApJ*, 707, 1691
- Baker, A. 2000, PhD thesis, Caltech
- Barberà, C., Athanassoula, E., & García-Gómez, C. 2004, *A&A*, 415, 849
- Barbosa, F., Storchi-Bergmann, T., Cid Fernandes, R., Winge, C., & Schmitt, H. 2006, *MNRAS*, 371, 170
- Barbosa, F., Storchi-Bergmann, T., Cid Fernandes, R., Winge, C., & Schmitt, H. 2006, *MNRAS*, 396, 2
- Barnes, J. 1989, *Natur*, 338, 123
- Bianchi, S., Guainazzi, M., & Chiaberge, M. 2006, *A&A*, 448, 499
- Bolatto, A., Wolfire, M., & Leroy, A. 2013, *ARA&A*, 51, 207
- Brightman, M., & Nandra, K. 2011, *MNRAS*, 414, 3084
- Buta, R. 1987, *ApJS*, 64, 383
- Buta, R., Ryder, S., Madsen, G., et al. 2001, *AJ*, 121, 225
- Cappellari, M. 2002, *MNRAS*, 333, 400
- Cecil, G. 1988, *ApJ*, 329, 38
- Chapman, S., Morris, S., & Walker, G. 2000, *MNRAS*, 319, 666
- Cid Fernandes, R., Gu, Q., Melnick, J., et al. 2004, *MNRAS*, 355, 273
- Cisternas, M., Gadotti, D. A., Knapen, J. H., et al. 2013, *ApJ*, 766, 50
- Clarke, C., Kinney, A., & Pringle, J. 1998, *ApJ*, 495, 189
- Comerón, S., Knapen, J., Beckman, J., et al. 2010, *MNRAS*, 402, 2462
- Crook, A., Huchra, P., Martimbeau, N., et al. 2007, *ApJ*, 655, 790
- Curran, S., Polatidis, A., Aalto, S., & Booth, R. 2001, *A&A*, 368, 824
- Dale, D., Sheth, K., Helou, G., Regan, M., & Hüttemeister, S. 2005, *AJ*, 129, 2197
- Davies, R., Förster Schreiber, N. M., Cresci, G., et al. 2011, *ApJ*, 741, 69
- Davies, R., Maciejewski, W., Hicks, E., et al. 2009, *ApJ*, 702, 114
- Davies, R., Mark, D., & Sternberg, A. 2012, *A&A*, 537, A133
- Davies, R., Müller Sánchez, F., Genzel, R., et al. 2007, *ApJ*, 671, 1388
- Davies, R., Thomas, J., Genzel, R., et al. 2006, *ApJ*, 646, 754
- Davis, T., Alatalo, K., Sarzi, M., et al. 2011, *MNRAS*, 417, 882
- de Vaucouleurs, G., de Vaucouleurs, A., Corwin, H., et al. 1991, *The Third Reference Catalogue of Bright Galaxies (RC3)* (New York: Springer)
- Diaz, R., & Dottori, H. 2013, *MSAIS*, 25, 37
- Díaz-Santos, T., Alonso-Herrero, A., Colina, L., et al. 2010, *ApJ*, 711, 328
- Dumas, G., Mundell, C., Emsellem, E., & Nagar, N. 2007, *MNRAS*, 379, 1249
- Duprie, K., & Schneider, S. 1996, *AJ*, 112, 937
- Emsellem, E., Monnet, G., & Bacon, R. 1994, *A&A*, 285, 723
- Engel, H., Davies, R. I., Genzel, R., et al. 2010, *A&A*, 524, 56
- Erwin, P. 2004, *A&A*, 415, 941
- Erwin, P., & Debattista, V. 2013, *MNRAS*, 431, 3060
- Erwin, P., & Sparke, L. 2003, *ApJS*, 146, 299
- Esquej, P., Alonso-Herrero, A., González-Martín, O., et al. 2014, *ApJ*, 780, 86
- Fathi, K., Beckman, J., Zurita, A., et al. 2007, *A&A*, 466, 905
- Fischer, T., Crenshaw, D., Kraemer, S., & Schmitt, H. 2013, *ApJS*, 209, 1
- Gallimore, J., Yzaguire, A., Jakoboski, J., et al. 2010, *ApJS*, 187, 172
- Ganda, K., Falcón-Barroso, J., Peletier, R., et al. 2006, *MNRAS*, 367, 46
- García, A. 1993, *A&AS*, 100, 47
- García-Gómez, C., Barberà, C., Athanassoula, E., Bosma, A., & Whyte, L. 2004, *A&A*, 421, 595
- Georgakakis, A., Gerke, B., Nandra, K., et al. 2008, *MNRAS*, 391, 183
- Gil de Paz, A., Boissier, S., Madore, B. F., et al. 2007, *ApJS*, 173, 185
- Giuricin, G., Marinoni, C., Ceriani, L., & Pisani, A. 2000, *ApJ*, 543, 178
- Griech, M., Mathur, S., Ghosh, H., & Ferrarese, L. 2011, *ApJ*, 731, 60
- Grouchy, R., Buta, R., Salo, H., & Laurikainen, E. 2010, *AJ*, 139, 2465
- Haan, S., Schinnerer, E., Emsellem, E., et al. 2009, *ApJ*, 692, 1623
- Haehnelt, M., & Rees, M. 1993, *MNRAS*, 263, 168
- Hess, K., & Wilcots, E. 2013, *AJ*, 146, 124
- Hickox, R., Mullaney, J., Alexander, D., et al. 2014, *ApJ*, 782, 9
- Hicks, E., Davies, R., Maciejewski, W., et al. 2013, *ApJ*, 768, 107 (Paper I)
- Hicks, E., Davies, R., Malkan, M., et al. 2009, *ApJ*, 696, 448
- Higdon, J., & Wallin, J. 2003, *ApJ*, 585, 281
- Ho, L. 2008, *ARA&A*, 46, 475
- Ho, L., Darling, J., & Greene, J. 2008, *ApJS*, 177, 103
- Horellou, C., & Combes, F. 2001, *Ap&SS*, 276, 1141
- Hunt, L., & Malkan, M. 2004, *ApJ*, 616, 707
- Iserlohe, C., Krabbe, A., Larkin, J., et al. 2013, *A&A*, 556, A136
- Kamphuis, J., & Briggs, F. 1992, *A&A*, 253, 335
- Kannappan, S., Guie, J., & Baker, A. 2009, *AJ*, 138, 579
- Karachentseva, V., Mitronova, S., Melnyk, O., & Karachentsev, I. 2010, *AstBu*, 65, 1
- Karouzos, M., Jarvis, M., & Bonfield, D. 2014, *MNRAS*, 439, 861
- Katkov, I., Moiseev, A., & Sil'chenko, O. 2011, *ApJ*, 740, 83
- Kauffmann, G., Heckman, T., Tremonti, C., et al. 2003, *MNRAS*, 346, 1055
- Keel, W., Chojnowski, S. D., Bennert, V. N., et al. 2012, *MNRAS*, 420, 878
- Kilborn, V., Forbes, D., Barnes, D., et al. 2009, *MNRAS*, 480, 1962
- Kinney, A., Schmitt, H., Clarke, C., et al. 2000, *ApJ*, 537, 152
- Knapen, J., de Jong, R., Stedman, S., & Bramich, D. 2003, *MNRAS*, 344, 527
- Kocevski, D., Faber, S. M., Mozena, M., et al. 2012, *ApJ*, 744, 148
- Koss, M., Mushotzky, R., Veilleux, S., et al. 2011, *ApJ*, 739, 57
- Krajnović, D., Cappellari, M., de Zeeuw, T., & Copin, Y. 2006, *MNRAS*, 366, 787
- Laine, S., Shlosman, I., Kanpen, J., & Peletier, R. 2002, *ApJ*, 567, 97
- Laurikainen, E., Salo, H., & Buta, R. 2004, *ApJ*, 607, 103
- Laurikainen, E., Salo, H., Buta, R., Knapen, J., & Comerón, S. 2010, *MNRAS*, 405, 1089
- Li, Z.-Y., Ho, L., Barth, A., & Peng, C. 2011, *ApJS*, 197, 22
- Lisenfeld, U., Braine, J., Duc, P.-A., et al. 2002, *A&A*, 394, 823
- Liszt, H., & Dickey, J. 1995, *AJ*, 110, 998
- Lotz, J., Jonsson, P., Cox, T., & Primack, J. 2008, *MNRAS*, 391, 1137
- Lutz, D., Maiolino, R., Spoon, H., & Moorwood, A. 2004, *A&A*, 418, 465
- Maciejewski, W., Teuben, P. J., Sparke, L. S., & Stone, J. M. 2002, *MNRAS*, 329, 502
- Maciejewski, W. 2004, *MNRAS*, 354, 892
- Marconi, A., Oliva, E., van der Werf, P., et al. 2000, *A&A*, 357, 24
- Markwardt, C. 2009, in *ASP Conf. Ser. 411, Astronomical Data Analysis Software and Systems XVIII*, ed. D. A. Bohlender, D. Durand, & P. Dowler (San Francisco, CA: ASP), 251
- Marquez, I., Durret, F., Masegosa, J., et al. 2004, *A&A*, 416, 475
- Martini, P., Dicken, D., & Storchi-Bergmann, T. 2013, *ApJ*, 766, 121
- Martini, P., Regan, M., Mulchaey, J., & Pogge, R. 2003, *ApJS*, 146, 353
- Mathur, S., Fields, D., Peterson, B., & Grupe, D. 2012, *ApJ*, 754, 146
- Mazzalay, X., Maciejewski, W., Erwin, P., et al. 2014, *MNRAS*, 438, 2036
- Mazzalay, X., Saglia, R. P., Erwin, P., et al. 2013, *MNRAS*, 428, 2389
- Meixner, M., Puchalsky, R., Blitz, L., Wright, M., & Heckman, T. 1990, *ApJ*, 354, 158
- Michel-Dansac, L., Duc, P.-A., Bournaud, F., et al. 2010, *ApJL*, 717, L143
- Moiseev, A., Valdés, J., & Chavushyan, V. 2004, *A&A*, 421, 433
- Moorwood, A., van der Werf, P., Kotilainen, J., Marconi, A., & Oliva, E. 1996, *A&A*, 308, L1
- Morelli, L., Pompei, E., Pizzella, A., et al. 2008, *MNRAS*, 389, 341
- Morganti, R., de Zeeuw, P. T., Oosterloo, T. A., et al. 2006, *MNRAS*, 371, 157
- Morris, S., Ward, M., Whittle, M., Wilson, A., & Taylor, K. 1985, *MNRAS*, 216, 193
- Mulchaey, J., Regan, M., & Kundu, A. 1997, *ApJS*, 110, 299
- Müller-Sánchez, F., Davies, R., Eisenhauer, F., et al. 2006, *A&A*, 454, 481
- Müller-Sánchez, F., Davies, R., Genzel, R., et al. 2009, *ApJ*, 691, 749
- Müller-Sánchez, F., Prieto, M. A., Hicks, E., et al. 2011, *ApJ*, 739, 69
- Mundell, C., James, P., Loiseau, N., Schinnerer, E., & Forbes, D. 2004, *ApJ*, 614, 648
- Mundell, C., Pedlar, A., Axon, D., Meaburn, J., & Unger, S. 1995, *MNRAS*, 277, 641
- Nagar, N., & Wilson, A. 1999, *ApJ*, 516, 97
- Neistein, E., & Netzer, H. 2014, *MNRAS*, 437, 3373
- Novak, G., Ostriker, J., & Ciotti, L. 2011, *ApJ*, 737, 26
- Novak, N., Thomas, J., Erwin, P., et al. 2010, *MNRAS*, 403, 646
- Ondrechen, M., Van der Hulst, J., & Hummel, E. 1989, *ApJ*, 342, 39
- Orban de Xivry, G., Davies, R., Schartmann, M., et al. 2011, *MNRAS*, 417, 2721
- Peeters, E., Spoon, H., & Tielens, A. 2004, *ApJ*, 613, 986
- Piqueras López, J., Davies, R., Colina, L., & Orban de Xivry, G. 2012, *ApJ*, 752, 47
- Riffel, R. A., Storchi-Bergmann, T., Dors, O., & Winge, C. 2009, *MNRAS*, 393, 783
- Riffel, R. A., Storchi-Bergmann, T., & Nagar, N. 2010, *MNRAS*, 404, 166
- Riffel, R. A., Storchi-Bergmann, T., & Winge, C. 2013, *MNRAS*, 430, 2249
- Rosario, D., Santini, P., Lutz, D., et al. 2012, *A&A*, 545, A45
- Rosario, D., Trakhtenbrot, B., Lutz, D., et al. 2013, *A&A*, 560, A72
- Ryder, S., Buta, R., Toledo, H., et al. 1996, *ApJ*, 460, 665

- Sakamoto, K., Okumura, S., Ishizuki, S., & Scoville, N. 1999, *ApJS*, **124**, 403
- Sandage, A. 1975, *ApJ*, **202**, 563
- Sani, E., Davies, R. I., Sternberg, A., et al. 2012, *MNRAS*, **424**, 1963
- Sarzi, M., Falcón-Barroso, J., Davies, R. L., et al. 2006, *MNRAS*, **366**, 1151
- Schawinski, K., Simmons, B., Urry, M., Treister, E., & Glikman, E. 2012, *MNRAS*, **425**, L61
- Schawinski, K., Urry, C. M., Virani, S., et al. 2010, *ApJ*, **711**, 284
- Schinnerer, E., Eckart, A., & Tacconi, L. 2000, *ApJ*, **533**, 826
- Schirmer, M., Diaz, R., Holmberg, K., Levenson, N., & Winge, C. 2013, *ApJ*, **763**, 60
- Schneider, S. 1989, *ApJ*, **343**, 94
- Schnorr-Müller, A., Storchi-Bergmann, T., Nagar, N., & Ferrari, F. 2014, *MNRAS*, **438**, 3322
- Sheth, K., Regan, M., Hinz, J. L., et al. 2010, *PASP*, **122**, 1397
- Shlosman, I., Peletier, R., & Knapen, J. 2000, *ApJL*, **535**, L83
- Sil'chenko, O., Moiseev, A., Afanasiev, V., Chavushyan, V., & Valdes, J. 2003, *ApJ*, **591**, 185
- Simões Lopes, R., Storchi-Bergmann, T., de Fátima Saraiva, M., & Martini, P. 2007, *ApJ*, **655**, 718
- Simpson, C., Wilson, A., Bower, G., et al. 1997, *ApJ*, **474**, 121
- Storchi-Bergmann, T. 2014, in IAU Symp. 303, The Galactic Center: Feeding and Feedback in a Normal Galactic Nucleus, ed. L. O. Sjurwerman, C. C. Lang, & J. Ott (Cambridge: Cambridge Univ. Press), 354
- Storchi-Bergmann, T., Simões Lopes, R., McGregor, P., et al. 2010, *MNRAS*, **402**, 819
- Struck-Marcell, C., & Higdon, J. 1993, *ApJ*, **411**, 108
- Sturm, E., González-Alfonso, E., Veilleux, S., et al. 2011, *ApJL*, **733**, L16
- Tamburro, D., Rix, H.-W., Walter, F., et al. 2008, *AJ*, **136**, 2872
- Terashima, Y., & Wilson, A. 2001, *ApJ*, **560**, 139
- Treister, E., Schawinski, K., Urry, M., & Simmons, B. 2012, *ApJL*, **758**, L39
- Ulrich, M.-H., Maraschi, L., & Urry, M. 1997, *ARA&A*, **35**, 445
- van den Bergh, S. 2002, *AJ*, **124**, 782
- van Driel, W., Rots, A., & van Woerden, H. 1988, *A&A*, **204**, 39
- Veilleux, S., Meléndez, M., Sturm, E., et al. 2013, *ApJ*, **776**, 27
- Villforth, C., Hamann, F., Rosario, D. J., et al. 2014, *MNRAS*, **439**, 3342
- Walter, F., Brinks, E., De Blok, W., et al. 2008, *AJ*, **136**, 2563
- Wei, L., Kannappan, S., Vogel, S., & Baker, A. 2010, *ApJ*, **708**, 841
- Westoby, P., Mundell, C., Nagar, N., et al. 2012, *ApJSS*, **199**, 1
- Wilcots, E. 2009, *AN*, **330**, 1059
- Young, L., Bureau, M., Davis, T. A., et al. 2011, *MNRAS*, **414**, 940